

Quantifying the Predictability of ENSO Complexity Using a Statistically

Accurate Multiscale Stochastic Model and Information Theory

Xianghui Fang^{1,2,3} and Nan Chen^{4*}

1. *Department of Atmospheric and Oceanic Sciences and Institute of Atmospheric Sciences,*

Fudan University, 220 Handan Rd., Shanghai 200433, China

2. *Innovation Center of Ocean and Atmosphere System, Zhuhai Fudan Innovation Research*

Institute, Zhuhai 518057, China

3. *Shanghai Scientific Frontier Base of Air-Sea Interaction, Shanghai 200438, China*

4. *Department of Mathematics, University of Wisconsin-Madison, Madison, WI, USA*

arXiv:2203.02657v1 [physics.ao-ph] 5 Mar 2022

*Corresponding author: Nan Chen, chennan@math.wisc.edu

ABSTRACT

8 An information-theoretic framework is developed to assess the predictability of ENSO complexity,
9 which is a central problem in contemporary meteorology with large societal impacts. The informa-
10 tion theory advances a unique way to quantify the forecast uncertainty and allows to distinguish the
11 predictability limit of different ENSO events. One key step in applying the framework to compute
12 the information gain representing the predictability is to build a statistically accurate dynamical
13 model. To this end, a recently developed multiscale stochastic model, which succeeds in capturing
14 both the large-scale dynamics and many crucial statistical properties of the observed ENSO com-
15 plexity, is incorporated into the information-theoretic framework. It is shown that different ENSO
16 events possess very distinct predictability limits. In addition to the ensemble mean, the ensemble
17 spread also has remarkable contributions to the predictability. While the information theory indi-
18 cates that predicting the onset of the eastern Pacific El Niños is challenging, it reveals a universal
19 tendency to convert strong predictability to skillful forecast for predicting many central Pacific
20 El Niños about two years in advance. In addition, strong predictability is found for the La Niña
21 events, corresponding to the effective discharge process. In the climate change scenario with the
22 strengthening of the background Walker circulation, the predictability of sea surface temperature
23 in central Pacific has a significant response with a notable increase in summer and fall. Finally,
24 the Gaussian approximation is shown to be accurate in computing the information gain, which
25 facilitates the use of more sophisticated models to study the ENSO predictability.

1. Introduction

El Niño-Southern Oscillation (ENSO) is the most significant interannual climate signal in the tropics (Philander 1983; Ropelewski and Halpert 1987; Klein et al. 1999; McPhaden et al. 2006). In the classical viewpoint, ENSO was often regarded as a phenomenon with cyclical attributes (Jin 1997), in which the positive and negative phases are El Niño and La Niña, respectively. Yet, ENSO is known to show a significant diversity and irregularity (Capotondi et al. 2015; Timmermann et al. 2018). Many studies have suggested that there are at least two types of ENSO (Ashok et al. 2007; Yu and Kao 2007; Kao and Yu 2009). Based on the features during their mature phase, they are named as the eastern Pacific (EP) and the central Pacific (CP) types when the largest sea surface temperature (SST) anomaly is located near the coast of the South America and the dateline region, respectively (Yu and Kao 2007; Kao and Yu 2009). In addition to these two major categories, different ENSO events exhibit diverse characteristics in spatial pattern, peak intensity, and temporal evolution, which is known as the ENSO complexity (Hayashi and Watanabe 2017; Timmermann et al. 2018; Boucharel et al. 2021).

Due to its crucial impacts on both the regional and the global climate, simulating and forecasting ENSO has long been a focus of research in related fields. Through unremitting efforts, considerable achievements have been made and a series of ENSO models with a hierarchy of complexity have been developed, including conceptual models (Schopf and Suarez 1988; Picaut et al. 1996; Jin 1997; Wang and Picaut 2004), simple models (Leeuwen 2002; Fang and Zheng 2018), intermediate complex models (Zebiak and Cane 1987; Battisti and Hirst 1989; Neelin and Jin 1993; Zhang et al. 2003; Thual et al. 2016) and general circulation models. These models can generally successfully forecast the typical indices of ENSO 6 to 12 months in advance, thereby providing a reliable

basis for many other climatic predictions that depend on the forecast of ENSO (Jin et al. 2008; Barnston et al. 2012).

In spite of these achievements, there is still an expectation to further improve the ENSO forecast skill. However, before that can be done, it is essential to quantitatively understand what is the upper limit of the forecast skill, i.e., the potential predictability of ENSO. Furthermore, in addition to the overall predictability, it is of more practical importance to explore the predictability of different types of the ENSO events due to the distinct features and impacts related to the ENSO complexity. Understanding the gap between the potential predictability and the prediction skill can provide guidelines to the improvement of the existing models and the current forecast methods. Such a study may also suggest that the efforts for further improving the forecast of certain types of the ENSO events is futile if they are inherently unpredictable. It is worthwhile to notice that the conventional time series based path-wise measurements for assessing the ENSO forecast skill, such as the anomaly correlation coefficient and the root-mean-square error (RMSE) of the ensemble mean time series, are not the most suitable metric for quantifying the predictability of ENSO. First, despite being able to reveal some qualitative information related to the predictability, such as the spring prediction barrier, it remains unclear from the results associated with these path-wise errors the exact upper limit of the forecast skill. Second, ENSO is intrinsically a chaotic (or turbulent) system, which means quantifying the forecast uncertainty is indispensable. However, the deterministic forecast (including the ensemble average) together with the path-wise measurements lacks the ability of the uncertainty quantification in the forecast, without which the meaning of the absolute path-wise error is less explainable for chaotic systems. Third, computing these path-wise skill scores requires a large number of data points, which often span for a long observational period. Thus, despite the possible ability to indicate certain overall characteristics, it is challenging to adopt these measurements for understanding the predictability of each individual ENSO event.

In this paper, an information-theoretic framework (DelSole 2004; Majda et al. 2005; Kleeman 2011) is developed that allows a systematic study of the potential predictability of the ENSO complexity. Fundamentally different from the deterministic methods, the information-theoretic framework exploits the statistical forecast to quantify the predictability of each individual event in a complex chaotic system. The indicator of the predictability within this framework is the time evolution of the information distance between the forecast distribution resulting from an ensemble forecast and the climatological one from the observational data. It denotes the additional information provided by the ensemble forecast that is beyond the prior known climatology, which is also called the information gain. Therefore, the information distance remaining in a high level suggests a long potential predictability. Similarly, the information distance rapidly decaying to zero implies that there is no need to run the model forecast beyond that point since the forecast becomes indistinguishable from the climatological distribution. It is notable that, if the information distance is near zero, then the ensemble mean forecast is expected to be close to the climatological mean, which often leads to an unskillful forecast in the path-wise sense as well. Thus, the predictability resulting from the information theory naturally provides an upper bound of the prediction skill, which satisfies the general definition of the predictability. There are several desirable features of adopting such an information-theoretic framework to understand the predictability of chaotic systems (Cover 1999; Kleeman 2002; DelSole and Tippett 2007), including the ENSO. First, as the focus of the framework is the entire distribution, which is also called the probability density function (PDF), the quantification of forecast uncertainty has been taken into account in the assessment of the predictability. This is vital for chaotic systems as each single forecast trajectory often deviates quickly from the truth. Second, in contrast to the calculation of the path-wise skill scores at a fixed lead time that requires a large number of the ensemble mean forecast results with different initializations, the information theory allows to quantify the predictability of a specific

event starting from a given initial condition. In fact, the forecast distribution at a fixed lead time can be formulated by the collection of different forecast ensemble members. Such a unique feature allows us to distinguish the predictability limit of different ENSO events, which is crucial for understanding and advancing the prediction of the ENSO complexity.

Although the concept of information theory has been proposed for decades, there exists a major barrier in applying the information theory to effectually quantify the predictability of many complex natural phenomena. In fact, the effectiveness of the resulting predictability from the information theory depends on the model that is utilized for the statistical forecast. A necessary condition of the reliable predictability provided by the information theory is the statistical accuracy of the forecast model. Otherwise, the model error rather than the intrinsic predictability may become the dominant component of the information distance (Giannakis and Majda 2012; Branicki et al. 2013; Chen and Majda 2016). However, reproducing the statistical features is often not the most primary focus of the existing dynamical models. Therefore, special cautions need to be paid for assessing the predictability when these models are incorporated into the information-theoretic framework. Although the information theory has been applied to study the basic overall El Niño predictability in the EP region (Tang et al. 2005) and leads to some interesting insights, it is unclear about the proportion of the explainable information gain there related to the actual predictability and due to the model error, respectively. On the other hand, some simple purely data-driven or statistical models, such as the linear regression models and the linear inverse models, are able to recover certain basic statistics, for example, the climatology covariance (Dominiak and Terray 2005; Alexander et al. 2008). However, the lack of the crucial nonlinear dynamics and explainable physics may also impede these models for characterizing the predictability of nature since the transient behavior using the purely data-driven models can be very different from that of the actual nonlinear chaotic systems.

To facilitate the quantification of the ENSO predictability within the information-theoretic framework, a recently developed conceptual multiscale stochastic model for the ENSO complexity is utilized in this study (Chen et al. 2022). To our knowledge, this is the first simple model that can accurately capture many desirable large-scale dynamical properties and statistical features of the ENSO complexity. The model starts with a deterministic three-region system for the interannual variabilities. Then two stochastic processes of the intraseasonal and decadal variation are incorporated. The model can reproduce not only the general properties of the observed ENSO events, but the complexity in patterns (e.g., CP vs. EP El Niño events), intensity (e.g., 10-20 year reoccurrence of extreme El Niños), and temporal evolution (e.g., more multi-year La Niñas than multi-year El Niños) as well. Notably, the model can also accurately simulate the PDFs, the power spectra and the seasonal phase-locking of the SST variations in both the CP and EP regions. In addition, the low computational cost of such a conceptual model allows us to use a large number of the ensembles for the study here, avoiding the statistical error due to the undersampling issue. Therefore, this model is a suitable candidate for us to explore the predictability of ENSO complexity from the perspective of the above mentioned information-theoretic framework. Notably, understanding the predictability of the ENSO complexity is a much more challenging but important task than studying the overall SST predictability in only the EP region.

The rest of this paper is organized as follows. The general framework of quantifying the predictability of complex natural phenomena using information theory is presented in Section 2. Section 3 introduces the datasets used in this study. It also includes a brief summary of the statistically accurate multiscale stochastic conceptual model. Section 4 presents the overall ENSO predictability while the predictability of different ENSO events related to the ENSO complexity is analyzed in Section 5. The sensitivity analysis, including the ENSO predictability in the climate

change scenarios and the role of each multiscale component in affecting the ENSO prediction, is investigated in Section 6. The conclusions and discussions are provided in Section 7.

2. An Information-Theoretic Framework: Quantifying the Predictability of Complex Natural Phenomena

We start with building the general framework of using information theory to quantify the predictability of complex natural phenomena, which will then be applied to the study of the ENSO complexity. The key quantities within the framework are a) the forecast PDF $p(t)$ from a suitable model, b) the initial value and the climatological PDF p_{clim} obtained from observational data, and c) a simple and effective approach to compute the information distance between $p(t)$ and p_{clim} . A schematic illustration of the framework is summarized in Figure 1, which contains four steps.

Step 1. Computing the climatological PDF p_{clim} and the temporal autocorrelation function (ACF) from observational data.

The observational climatological PDF p_{clim} plays a vital role, serving as a reference solution, in the study of the predictability via the information-theoretic framework. Given the observational data, say for simplicity an index (time series), the climatological PDF p_{clim} can be computed by first drawing the histogram from the data and then normalizing it. In practice, p_{clim} is often a time periodic function with period being one year, representing the seasonal cycle. Therefore, if a partition consisting of 12 equidistant points is used to formulate such a time-periodic function, then all the data corresponding to a specific month can be used to compute the associated climatological PDF for that month.

On the other hand, the ACF is not explicitly involved in computing the information gain for quantifying the predictability. Nevertheless, it is of fundamental importance in Step 2, serving as one of the central guidelines for the development of a statistically accurate dynamical model that is

used to compute the time evolution the forecast PDF $p(t)$. Autocorrelation is the correlation of a signal with a delayed copy of itself as a function of delay (Gardiner 2009). The ACF measures the overall memory of a chaotic system and describes the averaged convergence rate of the statistics towards the climatology. For a zero mean and stationary time series u , the ACF can be calculated as

$$\text{ACF}(t) = \lim_{T \rightarrow \infty} \frac{1}{T} \int_0^T \frac{u(t+t')u^*(t')}{\text{Var}(u)} dt'. \quad (1)$$

where t is the delay and T is the total length of the time series. The limit is taken for the mathematical rigor. In practice, the ACF is approximated by using a finite value of T in (1), provided that T is sufficiently large.

Step 2. Development of a statistically accurate dynamical model.

This is one of the most vital and challenging steps that involve the incorporation of important physics into the framework. In fact, the prerequisite of applying the information theory for the quantification of predictability is to develop a suitable model that provides the ensemble forecast PDF $p(t)$. The accuracy of the resulting information gain depends on the skill of such a model in reproducing nature. The calculated information gain is exact only when the perfect model of nature is adopted. Otherwise, the resulting information gain used to explain the predictability can be polluted by the model error. However, the perfect model is never known in practice. Therefore, to mitigate the error in computing the information gain, it is important to build a statistically accurate dynamical model for characterizing nature. Specifically, two necessary conditions have to be satisfied that facilitate the mitigation of the model error in calculating the information gain related to the predictability (Majda and Chen 2018; Majda and Qi 2018).

(a) Model fidelity: The model must have the skill to reproduce the climatological PDF of nature.

Such a necessary condition guarantees the consistency of the model at long lead times with the

observational statistics. If the model lacks the fidelity, then the information distance between $p(t)$ and p_{clim} at long lead time will never become zero. As a consequence, the predictability will become infinity, which is erroneous.

(b) Model memory: The model must be able to capture the overall temporal autocorrelation of nature. Satisfying the model fidelity guarantees the long-term statistics being captured. However, without additional constraints, the model fidelity itself is not sufficient to ensure that the time evolution of the statistics and the associated relaxation tendency towards the climatological distribution of the model are consistent with those of nature. In other words, the time evolution of the information gain computed from the model can be biased due to the failure of model in capturing the transient behavior of nature. Since the ACF measures the overall memory of a chaotic system, the difference between the temporal ACFs can be utilized as a simple and effective practical criterion to characterize the similarity of the transient behavior between the two systems. A suitable model that can be used for the information-theoretic framework should have the ACF that resembles the one of nature.

To provide intuitions, some illustrative example of the model fidelity and the model memory are included at the right top corner of Figure 1. The blue shading area represents the time evolution of the climatological PDF computed from observational data. The red shading area stands for the time evolution of the model PDF starting from a specific observed event, the actual time evolution of which is denoted by the black solid curve. The four rows show the results using different models. The model in the first row satisfies both the model fidelity and model memory since the time evolution of the model statistics tracks the observational trajectory and it converges to the same climatology as the observations. The models in the second and the third row also satisfy the model fidelity but the relaxation of the statistics towards the climatology are either much slower or much faster than that of nature for this given observed event. These two models fail to characterize the

overall memory of nature. The model in the last row has a consistent autocorrelation with nature but the variance of the climatological PDF is underestimated compared with nature, which means the model fidelity is not satisfied.

In practice, stochastic parameterizations and statistical closure approximations can be incorporated into the existing models to improve the statistical accuracy (Plant and Craig 2008; Gottwald and Harlim 2013; Berner et al. 2017; Christensen et al. 2017). The additional components can be calibrated by a certain optimization algorithm with the minimization of the error in the PDFs and ACFs being the cost function. This can be easily implemented for at least simple or conceptual models (Sapsis and Majda 2013; Chen et al. 2014a; Chen and Majda 2018).

Step 3. Ensemble forecast with a given initial value: aiming to obtain the forecast PDF $p(t)$ at different lead time t .

The forecast PDF $p(t)$ is computed by running the model repeatedly forward in time starting from a given initial condition from observations (with a slight perturbation if needed). Due to the random forcing or the intrinsic chaotic behavior of the model, different realizations will be distinct with each other. Collecting all the forecast realizations allows to form a forecast PDF $p(t)$ at each lead time t .

Step 4. Computing the information gain as a function of forecast lead time t .

With the observational climatological PDF p_{clim} and the time evolution of the forecast PDF $p(t)$ in hand from the previous steps, what remains is to develop an appropriate information criterion to compute the difference between $p(t)$ and p_{clim} . Such a difference represents the additional information in $p(t)$ beyond the observational climatology, which naturally reflects the potential predictability (Kleeman 2011; Buizza and Leutbecher 2015).

Since the comparison is two PDFs, the information theory is a more appropriate choice than the path-wise measurements. One natural way to assess the information gain in $p(t)$ compared with the climatological PDF p_{clim} is through the relative entropy $\mathcal{P}(p(t), p_{clim})$ (Majda et al. 2005; DelSole and Tippett 2007; Kleeman 2011),

$$\mathcal{P}(p(t), p_{clim}) = \int p(t) \log \left(\frac{p(t)}{p_{clim}} \right), \quad (2)$$

which is also known as Kullback-Leibler divergence or information divergence (Kullback and Leibler 1951; Kullback 1959, 1987). Despite the lack of symmetry, the relative entropy has two attractive features. First, $\mathcal{P}(p(t), p_{clim}) \geq 0$ with equality if and only if $p(t) = p_{clim}$. Second, $\mathcal{P}(p(t), p_{clim})$ is invariant under general nonlinear changes of variables. These provide an attractive framework for assessing the information gain as well as quantifying the model error and model sensitivity in other applications (Majda et al. 2002; Kleeman 2002; DelSole 2005; Tang et al. 2007; Branstator and Teng 2010; Teng and Branstator 2011; Giannakis and Majda 2012; Chen et al. 2014b; Liu et al. 2017).

One practical setup for utilizing the framework of information theory in many applications arises when both the measurements involve only the mean and covariance so that

$$p(t) \approx p^G(t) \sim \mathcal{N}(\bar{\mathbf{u}}, \mathbf{R}) \quad \text{and} \quad p_{clim} \approx p_{clim}^G \sim \mathcal{N}(\bar{\mathbf{u}}_{clim}, \mathbf{R}_{clim})$$

can be approximated by Gaussian distributions. In this case, $\mathcal{P}(p(t), p_{clim})$ has the explicit formula

$$\mathcal{P}(p(t), p_{clim}) = \left[\frac{1}{2} (\bar{\mathbf{u}} - \bar{\mathbf{u}}_{clim})^* \mathbf{R}_{clim}^{-1} (\bar{\mathbf{u}} - \bar{\mathbf{u}}_{clim}) \right] + \left[-\frac{1}{2} \log \det(\mathbf{R} \mathbf{R}_{clim}^{-1}) + \frac{1}{2} (\text{tr}(\mathbf{R} \mathbf{R}_{clim}^{-1}) - d) \right], \quad (3)$$

where \cdot^* is the transpose, \det is the determinant of a matrix, and d is the dimension of the state variable used to compute the relative entropy. In (3), the first term in brackets is called ‘signal’, reflecting the information difference in the mean but weighted by the inverse of the

climatological variance, \mathbf{R}_{clim} , whereas the second term in brackets, called ‘dispersion’, involves only the information distance regarding the covariance ratio, $\mathbf{R}\mathbf{R}_{clim}^{-1}$. The signal and dispersion terms in (3) are individually invariant under any (linear) change of variables which maps Gaussian distributions to Gaussians.

Note that, although the relative entropy has a lower bound 0 when $p(t) = p_{clim}$, it has no upper bound. For the convenience of presentation, a rescaled version of the relative entropy will be utilized in the remaining of the paper (Giannakis et al. 2012),

$$\mathcal{E} = 1 - \exp(1 - \mathcal{P}) \quad (4)$$

and therefore \mathcal{E} is scaled to the interval $[0, 1]$. The rescaled relative entropy \mathcal{E} is still a monotonically increasing function as the difference between $p(t)$ and p_{clim} . In the following, the relative entropy, together with its signal and dispersion components, refers to the rescaled version in (4). Such a rescaled information gain in (4) is served as the indicator of the predictability.

3. Observational Data Sets and the Statistically Accurate Model for the ENSO Complexity

a. Data

The monthly ocean temperature and current data are both from the GODAS dataset (Behringer and Xue 2004). The thermocline depth along the equatorial Pacific is approximated from the potential temperature as the depth of the 20°C isotherm. The analysis period is from 1982 to 2019. Anomalies presented in this study are calculated by removing the monthly mean climatology of the whole period. In this work, the Niño4 (T_C) and Niño3 (T_E) indices are the average of SST anomalies over the regions 160°E - 150°W , 5°S - 5°N (CP) and 150°W - 90°W , 5°S - 5°N (EP), respectively. The h_W index is the mean thermocline depth anomaly over the western Pacific (WP)

region (120°E - 180° , 5°S - 5°N) while the u index is the mean mixed-layer zonal current in the CP region.

The daily zonal wind data at 850 hPa from the NCEP–NCAR reanalysis (Kalnay et al. 1996) is used to depict the intraseasonal wind bursts. By removing the daily mean climatology, the wind burst index is obtained by averaging the anomalies over the WP region. Besides, the Walker circulation strength index is adopted to measure the effect of the decadal variation in the characteristics of ENSO. Based on the definition of Kang et al. (2020), it is defined as the sea level pressure difference over the CP/EP (160°W - 80°W , 5°S - 5°N) and over the Indian Ocean/WP (80°E - 160°E , 5°S - 5°N). Note that the monthly zonal SST gradient between the WP and CP region is highly correlated with this Walker circulation strength index (correlation coefficient of ~ 0.85), suggesting significant air–sea interaction over the equatorial Pacific. Since the latter is more directly related to the zonal advective feedback strength over the CP region, the decadal model (I) mainly illustrates this variable.

b. Definitions of different types of the ENSO events

To quantify the complexity of ENSO, the definitions of different El Niño and La Niña events are as follows [based on the average SST anomalies during boreal winter (December–January–February; DJF)]: Following the definition in Kug et al. (2009), when the EP is warmer than the CP and is greater than 0.5°C , it is classified as the EP El Niño. Among this, based on the definitions used by Wang et al. (2019), an extreme El Niño event corresponds to the situation that the maximum of EP SST anomaly from April to the next March is larger than 2.5°C . When the CP is warmer than the EP and is larger than 0.5°C , the event is then defined as a CP El Niño. Finally, when either the CP and EP SST anomaly is cooler than -0.5°C , it is defined as a La Niña event.

c. The multiscale stochastic model for ENSO complexity

In this work, a multiscale stochastic conceptual model is used to study the predictability of ENSO complexity, which was recently developed in Chen et al. (2022). This is a three-region model, aiming to reproduce the observed dynamical and statistical features in both the CP and EP regions. The combination of suitable stochastic parameterizations with nonlinear interactions between interannual, intraseasonal and decadal variabilities allows the model to generate different types of the observed ENSO events. As is shown in Chen et al. (2022), this model succeeds in capturing the large-scale ENSO complexity and the associated statistics. Here, we briefly summarize the main components of this model, while more details can be found in the original paper.

The model starts with a deterministic, linear and stable system for the interannual variabilities (Fang and Mu 2018). It is a general extension of the classical recharge oscillator model (Jin 1997) and depicts the air-sea interactions over the entire WP, CP and EP. That is, it includes both the ocean heat content discharge/recharge and the ocean zonal advection. Then, two stochastic processes with multiplicative noise describing the intraseasonal wind bursts and the decadal variation in the Walker circulation are incorporated to depict ENSO's irregularity and the decadal variation in the strength and occurrence frequency of EP and CP El Niño events (Timmermann et al. 2018; Fang and Xie 2020). The model reads:

$$\frac{du}{dt} = -ru - \frac{\alpha_1 b_0 \mu}{2} (T_C + T_E) + \beta_u \tau + \sigma_u \dot{W}_u, \quad (5a)$$

$$\frac{dh_W}{dt} = -r h_W - \frac{\alpha_2 b_0 \mu}{2} (T_C + T_E) + \beta_h \tau + \sigma_h \dot{W}_h, \quad (5b)$$

$$\frac{dT_C}{dt} = \left(\frac{\gamma b_0 \mu}{2} - c_1(T_C) \right) T_C + \frac{\gamma b_0 \mu}{2} T_E + \gamma h_W + \sigma u + C_u + \beta_C \tau + \sigma_C \dot{W}_C, \quad (5c)$$

$$\frac{dT_E}{dt} = \gamma h_W + \left(\frac{3\gamma b_0 \mu}{2} - c_2 \right) T_E - \frac{\gamma b_0 \mu}{2} T_C + \beta_E \tau + \sigma_E \dot{W}_E \quad (5d)$$

$$\frac{d\tau}{dt} = -d_\tau \tau + \sigma_\tau(T_C) \dot{W}_\tau, \quad (5e)$$

$$\frac{dI}{dt} = -\lambda(I - m) + \sigma_I(I) \dot{W}_I. \quad (5f)$$

Here, the interannual component, i.e., Eqs. (5a)-(5d), depicts the main dynamics for both the CP and EP types of ENSO; the intraseasonal equation, Eq. (5e) represents the amplitude of the random wind bursts (τ); and the decadal part, Eq. (5f) represents the variation in the strength of the background Walker circulation (I). In the model, T_C and T_E are the SST in the CP and EP, u is the ocean zonal current in the CP and h_W is the thermocline depth in the WP. As was discussed in Chen et al. (2022), I also stands for the zonal SST difference between the WP and CP, which directly determines the strength of the zonal advective feedback. The parameter m is the mean of I , which can be computed from its PDF.

In this model, the stochasticity plays a crucial role in coupling variables at different time scales and parameterizing the unresolved features in the model. First, the intraseasonal variation τ is depicted by a simple stochastic differential equation, Eq. (5e) with a state-dependent (i.e., multiplicative) noise coefficient σ_τ , where \dot{W}_τ is a white noise source. τ is then coupled to the processes of the interannual part serving as external forcings. In addition, four Gaussian random noises $\sigma_u \dot{W}_u$, $\sigma_h \dot{W}_h$, $\sigma_C \dot{W}_C$ and $\sigma_E \dot{W}_E$ are further added to the processes describing the interannual variabilities, which effectively parameterize the additional contributions that are not explicitly modeled, such as

the subtropical atmospheric forcing at the Pacific Ocean and the influences from the other Ocean basins. In a more general sense, these stochastic noises can be regarded as the simplest way for stochastic parameterization, which increases the model variability such that the PDFs of the model variables can better match those of the observational data (Palmer et al. 2009). Second, since the details of the background Walker circulation consist of uncertainties and randomness (Chen et al. 2015), a simple but effective stochastic process is used to describe the temporal evolution of the decadal variability I (Yang et al. 2021), where \dot{W}_I in Eq. (5f) is another white noise source. The multiplicative noise in the process of I is aimed at guaranteeing the positivity of I due to the fact that the long-term average of the background Walker circulation is non-negative. Besides, the effects of seasonality are added to both the wind activity and the collective damping to depict the seasonal phase-locking characteristics realistically, which manifests as the tendency of ENSO events to peak during boreal winter (Tziperman et al. 1997; Stein et al. 2014; Fang and Zheng 2021).

The dimensional units and the parameters in the coupled model are summarized in Table 1.

d. The dynamical and statistical features of the model

As was studied in Chen et al. (2022), this model can reproduce many desirable dynamical and statistical features of the observed ENSO complexity. Figure 2 illustrates a comparison between the model simulations and the observations. Panels (a)–(b) include the Hovmoller diagrams of the SST, which are reconstructed by a bivariate linear regression, where the regression coefficients at each longitude is provided by computing the correlations of its SST value with the time series of T_E and T_C , respectively (Chen et al. 2022). These two panels reveal that the model can reproduce different types of the ENSO events with distinct locations, amplitudes, and durations, as are observed in nature. Panels (c)–(j) compare the model statistics with the observations in both the CP and the EP regions. The skillful recovery of the non-Gaussian climatological PDFs and the

ACFs indicates that the model satisfies both the necessary conditions in the information-theoretic framework, namely the model fidelity and the model memory. In addition, the observed power spectrum and the seasonal phase-locking features are captured by the model. Therefore, the model utilized here is statistically accurate and involves the basic large-scale dynamical features of the ENSO complexity, which provides a reasonable justification for applying it to the study of the predictability within the information-theoretic framework.

Before analyzing the predictability of ENSO complexity utilizing the information-theoretic framework, it is necessary to conduct a simple test of the model's representation of the observational forecast errors. To do this, a 2000-year long model simulation is generated and it is divided into 54 non-overlapping segments, each of which has the same length of time as the observations, i.e., 1982–2019. For each segment, we forecast T_E and T_C based on 100 ensembles. For observations, we use the observed u , h_W , T_C , T_E , τ and I as the initial values, while for different model segments the corresponding exact values from the simulation are utilized as the initialization. Figure 3 shows the forecast error for each segment (including the observation), i.e., the RMSE between the forecast ensemble mean and the true fields. It is seen that there is no significant difference in the forecasting ability of ENSO between the observation and model simulations for both T_E and T_C . That is, the longer bars corresponding to the observations are all covered by the mean and one standard deviation of the statistics obtained from the model segments. The results here suggest that the model is also capable of producing very realistic ENSO properties from a forecasting perspective, which further strengthens the justification of utilizing the model in studying the predictability of the ENSO complexity.

4. The Overall ENSO Predictability

a. The overall predictability, its Gaussian approximation, and the signal-dispersion decomposition

Figures 4 and 5 show the information gain of T_E and T_C , respectively, as a function of the starting date (x-axis) and the lead time (y-axis). The calculation of the information gain follows the information-theoretic framework developed in (2). An ensemble forecast by running the multiscale stochastic model (5) forward is utilized to compute the time evolution of the PDF, where the observation data of all the six variables are directly adopted as the initial value for the ensemble forecast. Since the model is a low-dimensional system, a large number of the ensembles containing 2000 members is utilized in the ensemble forecast, which ensures that the sampling error due to the insufficient ensemble number is negligible. The one-dimensional marginal distribution of T_E and T_C is utilized, respectively, in Figures 4 and 5 for computing the information gain from the formula in (4). The same setup is adopted in Section 5 when the predictability of different types of the events is studied. In Figures 4 and 5, the solid red line, purple line and blue line at the top of each panel mark the years with EP El Niño, CP El Niño and La Niña, respectively. To clarify the definition of “an(a) EP El Niño/CP El Niño/La Niña year”, an entire calendar year is treated provided that such an event is observed in the year even if it lasts only for a couple of months (especially at the end of the year corresponding to the boreal winter). The following conclusions can be drawn from these two figures.

First, the time evolution of the information gain, namely the predictability, varies significantly as the starting date. In particular, the predictability limit of the events starting from a La Niña year is longer than those starting from both the CP and the EP El Niño years. Yet, different individual events display distinct predictability limits. Such a finding has a remarkable significance for the study of the predictability of ENSO. It implies that it is too crude to employ a single value of the

predictability limit for the entire ENSO, which is however what the path-wise measurements can often provide for assessing the ENSO forecast skill by averaging over the entire testing period. Instead, it is anticipated that the ENSO predictability needs to be quantified for each individual event related to the ENSO complexity. The details will be analyzed in Section 5.

Second, comparing Panel (a) in the two figures, it can be seen that T_C overall has more predictability than T_E . This is somewhat counterintuitive as the strength of the CP events is often weaker than that of the EP ones. However, special cautions need to be paid here: EP events and CP events do not solely correspond to T_E and T_C . In fact, both events have composited variations of T_E and T_C . The reason for the stronger predictability of T_C is that its time series has a stronger temporal correlation than that of T_E (see Figure 2), indicating a potential to have a stronger predictability limit. In fact, it has been shown that the skillful prediction (above the threshold of pattern correlation = 0.5) remains at a longer lead time in predicting T_C than T_E (Ren et al. 2019; Wang et al. 2020).

Third, comparing Panels (a) and (b) in both figures, the Gaussian approximation seems to be an efficient and accurate simplification in computing the information gain, which is consistent with the finding in an earlier work that studied the SST in the EP region (Tang et al. 2005). Such a conclusion has a profound influence on applying the information theory to studying the ENSO predictability based on more sophisticated models, in which only a small number of the ensembles is affordable. A small ensemble size is often insufficient to recover the entire non-Gaussian PDF especially for high dimensional systems but it may provide a reasonably accurate Gaussian approximation of the PDF (Gardiner 2009). Yet, it is important to highlight that the skillfulness of the Gaussian approximation only implies that the information gain due to the higher order statistics behaves in a similar way as that from the mean and the variance. It does not suggest a linear model with Gaussian statistics is sufficient for the study of the predictability here. In fact, the information difference between the non-Gaussian climatological PDF with the optimal Gaussian approximation

is quite significant, which means a linear model with Gaussian statistics will violate the model fidelity to a large extent. Nevertheless, the high similarity between the total information gain and its Gaussian fit allows us to simply consider the latter in the remaining of the paper, which also facilitates the discussions with its signal-dispersion decomposition.

Finally, from the signal-dispersion decomposition of the information gain, it can be concluded that the signal part dominates the total information gain in T_C while both the signal and dispersion parts have remarkable contributions to T_E . Note that the latter is different from the qualitative conclusion in Tang et al. (2005), possibly because the model fidelity was not fully taken into account in that earlier work. The significant contribution from the dispersion part also indicates the importance of considering the entire forecast ensembles in characterizing the predictability instead of focusing on only the ensemble mean that merely impacts the signal part of the total information gain.

b. The predictability as a function of the starting month

Figure 6 shows the predictability performance of T_E and T_C as a function of the starting month. The results confirm that T_C has overall a stronger predictability than T_E and its main contributor is the signal part while the dispersion is a non-negligible component for predicting T_E . One particularly interesting finding from this figure is related to the well-known spring prediction barrier problem in many practical model forecasts and the persistence, which says the ENSO forecast skill drops significantly when straddling boreal spring. Yet, from the perspective of information theory, the forecast around spring does not demonstrate any significant barrier. On the contrary, the overall predictability is even longer for the events starting from the spring season, especially the SST in the CP region. This indicates that if accurate and proper information can be obtained around spring, there might be a potential to make meaningful ENSO forecasts at long lead times, beyond the

information provided by the climatology. Such a conclusion is also consistent with the results in a recent study (Fang and Zheng 2021).

To further understand the difference in the ENSO predictability with different initial conditions, the three columns of Figure 7 show the information gain in predicting T_E and T_C starting from those dates, which belong to the EP El Niño years, the CP El Niño years and the La Niña years, respectively (see the bars at the top of each panel in Figure 4 or 5). The additional messages provided by Figure 7 is as follows. First, a stronger predictability is observed if the forecast starts from a La Niña year than a year with either type of the El Niño, especially when the starting date ranges from January to June. The contribution from these La Niña years accounts for the overall stronger predictability in the spring season, as was shown in Figure 6, since the results associated with the El Niño events are the opposite. The stronger predictability starting from a La Niña year is probably related to the more effective discharge process of El Niño at its mature stage (Planton et al. 2018). Quantitatively, El Niño has a predictability of 6–10 months in general, while La Niña has a much longer one, which can often exceed two years. Such a finding suggests that there remains a potentially large gap between our current level of ENSO forecast and its predictability, which has a room for the further improvement. Second, it is noticed that the information gain of T_C (red curves) starting from the second half of the year for both the EP and CP El Niño years has a clear reemergence. This is mainly related to the climatological PDF structure of T_C , that is, the PDF of T_C is more concentrated around the mean than that of T_E during summer and autumn. In other words, the variance of T_C is smaller than that of T_E during those seasons (see Panels (g)–(h) in Figure 2). For the El Niño forecast starting from the second half of the year, it tends to become a La Niña event due to its effective discharge process, where the center of the anomalous SST is often closer to the CP. As a consequence, the ensembles have a negative mean value of T_C , which leads to a large difference compared with the climatological PDF. This explains the reemergence

of the information gain. Third, comparing the two types of the El Niño events, the EP type of El Niño shows a stronger reemergence at the longer lead time for the forecast that begins in the fall or winter than the CP events. In addition, the EP type of El Niño generally has a slightly stronger predictability than the CP type. This is consistent with our intuition since the EP type of the El Niño usually has stronger amplitude. It is also not contradictory with the conclusion drawn from Figures 4–5 that T_C overall has stronger predictability than T_E .

5. Predictability of Different ENSO Events Consisting of the ENSO Complexity

Figures 8, 12 and 14 show the information gain in predicting 7 different ENSO events that consist of the ENSO complexity: 1) a moderate EP El Niño (1986-1988), 2) a super El Niño (1997-1998), 3) a delayed super El Niño (2014-2016), 4) an isolated CP El Niño (2004-2005), 5) a mixed CP-EP El Niño (2009-2010), 6) a single-year La Niña (1988-1989) and 7) a multi-year La Niña (1999-2000). See Section b for the definitions of these events. In these figures, the x-axis is the starting date while the y-axis is the forecast lead time in the unit of month. The two white solid lines provide the time window within which the corresponding event is active.

a. Moderate EP El Niño, super El Niño and delayed super El Niño

First, according to Figure 8, the information gain along the first white solid line for all the three EP El Niño events decays to zero very quickly, which indicates that it is very challenging to predict the onset phase of the EP El Niño events. In fact, the westerly wind bursts are believed to be one of the major triggering effects of the EP El Niño events (Harrison and Vecchi 1997; Tziperman and Yu 2007; Puy et al. 2016). However, the wind bursts lie in the intraseasonal time scale and are inherently hard to be forecasted in the interannual time scale. This leads to the intrinsic difficulty in effectively predicting the onset of the EP El Niño.

In addition to the common features in the predictability of all the three EP El Niño events, there are also some differences between them. Column (a) of Figure 8 shows the predictability of the 1986-1988 moderate EP El Niño event. When the starting date is at the growing phase of the event (i.e. October 1986 to March 1987), the significant value of the information gain maintains only for about 6 months. When the starting date is after the event peak, i.e., July 1988, the predictability starts to become longer. This is because the initial value of the SST at these time instants is stronger than the climatological mean value, which provides additional important information that facilitates the prediction. One notable finding is that, if the starting time is between July 1988 to January 1989, then the information gain of T_C within the first 10 months is close to zero. Nevertheless, the information gain has a significant increase afterwards and peaks at the lead time of about 15 to 20 months. Such a peak time undoubtedly corresponds to the subsequent La Niña event. The predictability is related to the effective discharge process. The time span before the information gain reemergence corresponds to the phase change time from El Niño to La Niña and the time for the information passing from the EP region to the CP area. Different from the moderate EP El Niño event, Column (b) shows that starting from both the growing phase (April) and the mature phase (October) of the 1997-1998 super El Niño, the information gain is significant for more than 10 months, though the gain is more pronounced for a short lead time in the latter case which is expected. This indicates the potentially stronger predictability of super El Niño than the moderate events, even starting from the late spring season, which is also consistent with the current prediction skill using various models.

Column (c) of Figure 8 shows the result of the 2014-2016 delayed super El Niño. It can be seen that the predictability reaches a local peak if the starting date is around July 2014, which corresponds to the mature phase of the moderate El Niño event in this three-year episode. Then regarding the subsequent super El Niño in 2015, the information gain has a similar tendency as

that in 1997-1998. The only difference is that the information gain of the 2015 event seems to be sensitive to the starting date. Specifically, the information gain remains significant if the starting date is April or June 2015 while the gain is consistently tiny regardless of the forecast lead time if the starting date is March, May or July. This is related to the rapid change of the wind bursts in 2015, which is one of the main triggering effects of the super El Niño (Chen et al. 2015; Hu and Fedorov 2016; Thual et al. 2019; Xie and Fang 2020). In fact, as is shown in Figure 9, the westerly wind bursts suddenly disappear in 2015 May while other variables stay in the consistent states. As a consequence, there is no mechanism in lifting the ensemble members towards extreme values, which can be seen in Column (c) of Figure 10. The Hovmoller diagram in Figure 11 validates such a finding. It also shows that the reconstructed spatiotemporal pattern is poorly predicted starting from May 2015 in the ensemble mean forecast while the forecast is much more accurate if the starting date is either April or June. Note that the ensemble forecast PDF starting from March or May 2015 relaxes quickly towards the climatology while that starting from April or June is very distinguishable from the climatological PDF with the help of the strong wind bursts that also account for a large percentile of the ensemble members to forecast the 2015 super El Niño event. These ensemble evolutions explain the sawtooth profile in Column (c) of Figure 8 for the predictability and links the forecast skill with the predictability.

Finally, it is noticeable that, the predictability of T_E extends further in time than that of T_C for all the three types of the EP El Niño events when the starting date is before or during the events. This seems to reach an opposite conclusion compared with the overall predictability shown in Figures 4–5, which says T_E has a weaker potential predictability than T_C . Yet, as was discussed in the previous section, the latter is due to the large contribution from the La Niña events. Therefore, such a comparison again highlights the large discrepancy in the predictability of different types of the ENSO events and indicates necessity of studying each type of the events.

b. Isolated CP El Niño and mixed CP-EP event

Column (a) in Figure 12 shows the predictability of a single-year (or isolated) CP event in 2004-2005 while Column (b) displays that of a mixed CP-EP event in 2009-2010. When the forecast starts from anytime during the single-year CP event, the predictability remains quite weak. This is not surprising since the SST anomaly for most of the CP events is not as strong as the EP ones and therefore the additional information provided by the initial condition dissipated within a short time. In contrast, the predictability is more pronounced for the mixed CP-EP event, in which the strong EP SST contributes to the overall predictability and the information passes from the EP to the CP region.

In addition to these basic discoveries, there is one very interesting finding for both the events. That is, starting from about 20 months in advance (January 2003 and May 2008 respectively), the information gain can tell that the ensemble forecast distribution at the CP event peak is significantly different from the climatological PDF. Notably, this is not observed in the EP El Niño or La Niña events (Figures 8 and 14) and it seems to be a unique feature of the CP El Niño. Although a large information gain does not necessarily guarantee an accurate forecast, it does imply the forecast contains additional information beyond the climatology. In other words, there could be a potential to predict the occurrence of the CP events about two years in advance if suitable improvement is implemented in the current forecast systems.

To understand if the information gain remaining significant at the 20-month lead time is a universal characteristic for all CP events, Figure 13 shows the information gain in predicting T_C for 6 different CP El Niño or CP-EP mixed events, which are marked next to the Hovmoller diagram in Panel (a). Among these 6 events, shown in Panels (b)–(g), 4 of them clearly demonstrate such a feature; they are the one in years 1994-1995, 2002-2003, 2004-2005 and 2009-2010. The CP

event during 2018-2019 also reveals a tendency of the predictability at this long lead time, although the information gain is quite weak. On the other hand, the CP event during 1991-1992 does not display strong predictability. However, the warm SST center of the 1991-1992 event locates more towards the EP region compared with the other CP events, which might be the reason for the distinct behavior of the information gain of this event. Panels (h)–(j) show the ensemble forecast for the 1994-1995, the 2002-2003, and the 2009-2010 events. Clearly, the ensembles at a lead time around 20 months is quite distinguishable from the climatology, which confirms a large information gain. However, it is worthwhile to highlight again from these results that the predictability does not necessarily mean the skillful prediction. In fact, despite a large information gain, the ensemble mean time series is far from the observations during 1994-1995 event in Panel (h). Fortunately, the observed event is still captured by some ensemble members. Therefore, if a large information gain is obtained, then it is justified to conclude the forecast is distinguishable from the climatology while each plausible event from the forecast is assigned with a certain probability. On the other hand, the ensemble evolutions in Panel (i) show a skillful forecast for the 2002-2003 event, converts the predictability to the actual prediction skill, while those in Panel (j) also accurately predict the occurrence of the 2009-2010 CP El Niño.

c. Single-year and multi-year La Niñas

The predictability of a single year La Niña event (1988-1989) and a multi-year La Niña event (1998-2001) is shown in Figure 14. The results here confirm the conclusion discussed in the previous section that the La Niña events usually have stronger predictability since they are the discharge phase of the ENSO cycle. One interesting finding in the 1988-1989 single-year La Niña event is that the bound of the significant value of the information gain is consistent with the La Niña's demise (the white line). This implies the forecast ensembles reaching the climatological

PDF is in phase with the relaxation of the La Niña towards the quiescent state. Such a finding indicates that this La Niña event follows exactly the discharge-recharge paradigm and is therefore predictable. On the other hand, the 1998-2001 multi-year La Niña shows a strong predictability when the forecast begins from either the preceding El Niño event, even with the spring starting time, or the onset of the negative SST phase (middle of year 1998). The information gain decays as the starting time becomes 1999 or 2000, at which the amplitude of the initial value becomes weak.

Finally, Figure 15 includes some intuitive results. It shows the ensemble forecast of the 1998-2001 multi-year La Niña and the 2004-2005 isolated CP El Niño. As is shown in Column (a), starting from January 1998, the ensembles of T_C for the 1998-2001 event evolve in a very different way from the climatological PDF for more than two years, which accounts for the large information gain as was shown in Panel (a) of Figure 14. In fact, the ensemble mean here also tracks the truth in an accurate fashion. Thus, the strong predictability in such a situation indeed converts to the skillful forecast. On the other hand, as is shown in Column (b), the initial values of both T_E and T_C at January 2004 are close to zero and the ensembles spread quickly towards the climatology as well. In such a case, despite that the time series of the true event is consistently included within the ensemble spread, the forecast ensembles cannot effectively provide any useful additional information beyond the climatology.

6. Sensitivity Analysis

a. ENSO predictability in the climate change scenarios

Recall, in the multiscale stochastic model (5), the variable I represents the background dynamic Walker circulation and varies in the decadal time scale. One important practical issue is to understand the ENSO predictability in the climate change scenarios, which can be implemented by

perturbing I in the model. The study in this subsection is based on perfect model twin experiments with different choices of the decadal variability I . The perfect model twin experiments mean the model is first used to generate synthetic time series as “observations” and then the same model is used for quantifying the predictability. The reason to exploit the perfect model twin experiment is that the observational data of the possible future climate change scenario are not available. Since the model has been shown to be statistically accurate and the predictability of the model-generated time series has been validated to resemble that of the observations under the current climate (not shown here), the perfect model twin experiments are expected to at least provide some qualitatively useful conclusions. In the following, three perfect model twin experiments are carried out:

- (a) The current climate scenario. This is the standard run of the full model (5) with the standard parameters that captures the current climate statistics, where I is driven by the stochastic process (5f) and ranges from 0 to 4.
- (b) The climate scenario with the strengthening of the Walker circulation. In this scenario, the variable I is set to be a constant $I = 4$ in the model (5) and the stochastic process (5f) is discarded.
- (c) The climate scenario with the weakening of the Walker circulation. In this scenario, the variable I is set to be a constant $I = 0$ in the model (5) and the stochastic process (5f) is discarded.

The main results are illustrated in Figure 16. Panel (a) shows the number of different ENSO events occurred per 70 years. To include the uncertainty quantification, the confidence intervals are also added to the bar plots. These confidence intervals are computed based on 30 independent model simulations, each of which is 70-year long as the observations from 1950 to 2020. As a further validation of the model, the occurrence frequency of each type of the ENSO events from the

standard model run is compared with the observations under the current climate scenario. Despite a slight overestimation of the La Niña events in the model, the occurrence frequencies of all the other types of the events from the model match the observations very well, including the overall El Niño events, the CP events, the EP events, the extreme El Niño events, the multi-year events for both El Niño and La Niña. These comparisons provide reasonable justifications of utilizing the perfect model twin experiments to study the predictability in the climate change scenarios.

Panel (a) also shows that, with the strengthening of the background Walker circulation, the occurrence of the El Niño events increases while that of the La Niña decreases. Among different types of the El Niño events, the occurrence of the CP El Niño turns into more frequent while the extreme EP events become seldom to happen. On the other hand, although the total number of the La Niña events decreases, the frequency of the multi-year La Niña occurrence remains the same as the current climate. Therefore, according to the analysis of the predictability of the ENSO complexity in Section 5, it is anticipated that the predictability of T_C should increase as I becomes large while that of T_E remains at the same level as in the current climate. This conjecture is confirmed by Panels (b) and (d). In particular, the extended predictability of T_C is mainly observed in summer and fall seasons. In addition, the predictability of T_E is overall unchanged, although a slightly increment of the dispersion part is found. Similarly, if the dynamic Walker circulation is constantly weakened (with $I = 0$), then the predictability of T_C decreases, especially in spring and fall (Panel (c)), while that of T_E does not have obvious changes.

To summarize, in the climate change scenarios, the predictability of T_C has the most significant response. When the background Walker circulation becomes stronger (weaker), the predictability of T_C increases in summer and fall (decreases in spring and summer), while the predictability of T_C in winter and that of T_E throughout the year remains almost unchanged.

b. Role of the multiscale components in affecting the ENSO prediction

The focus of this subsection is on studying the influence of different model variables on the ENSO forecast, especially those that are not included in the classic recharge-discharge theory but play a crucial role in ENSO complexity. These variables include the intraseasonal zonal wind stress τ , the decadal variable I (proportional to the strength of the zonal advective feedback), and the zonal current u .

Such a study can also naturally fit into the information-theoretic framework with a slight rearrangement of the PDFs in computing the information distance,

$$\mathcal{P}(p_{reduced}(t), p(t)) = \int p_{reduced}(t) \log \left(\frac{p_{reduced}(t)}{p(t)} \right). \quad (6)$$

In (6), the reference solution $p(t)$ is the standard run of the ensemble forecast utilizing the full model (5) while the PDF $p_{reduced}(t)$ comes from running a “reduced model” in which one of the above mentioned variables is set to be zero. Then the information difference from (6) (after rescaling using (4)) is the information loss by ignoring the contribution from the specific variable.

Figure 17 shows the information loss by in the absence of the intraseasonal zonal wind stress τ . It has been pointed out that the wind bursts are crucial to the ENSO development, especially to the SST in the EP region (Harrison and Vecchi 1997; Tziperman and Yu 2007; Puy et al. 2016). This is confirmed by the information theory, where an enormous information loss is found by ignoring τ in the model ensemble forecast. Notably, the composites of the loss of information in predicting T_E and T_C are very different. The loss of information is mainly on the dispersion part for predicting T_E , which means the ensemble spread is significantly underestimated. Therefore, although the EP SST is dominated by the interannual air–sea interactions, the intraseasonal information provides as a supply by the up-scale cascade. This also indicates that a large portion of the variability in T_E comes from τ . In other words, τ triggers many events in the EP area, especially the extreme El

Niños (Hu and Fedorov 2016). On the other hand, despite the role of τ on T_C is not as strong as that on T_E , it still has a pronounced impact on the information gain in the CP area. Different from the prediction of T_E , the information loss in predicting T_C by excluding τ is mainly reflected in the signal part. This implies the random wind bursts can influence the deterministic component of the dynamics of T_C and lead to a mean bias in the forecast.

Next, Figure 18 explains the impact of the decadal variability I on the ENSO predictability. It is seen that I modifies both T_E and T_C with a significant and synchronized decadal variation feature. In particular, strong influence of I on the SST is found around 2000, 2010 and 2018, which are the years with La Niña and CP El Niño events. Therefore, although the ENSO events lie in the interannual time scale, the decadal variability is important for improving the predictability of ENSO in both CP and EP regions.

Finally, the loss of information by excluding the contribution from the zonal current u in the CP is shown in Figure 19. The loss of information caused by ignoring u in the forecast system is similar to that by disregarding the contribution from the decadal variability I , except that the influence of u on the ensemble prediction is mainly found in the CP region. In fact, u and I are strongly correlated in driving the time evolution of T_C . Since u is one of the main driven mechanisms of the CP El Niño events, it has a direct contribution to the SST in CP area. On the other hand, the contribution of u to the La Niña is not as significant as that of I . Taking into account both Figures 18 and 19, it can be concluded that, in the period of weak I that leads to a minor contribution from the ocean zonal current, ENSO's development can be effectively described by only considering the vertical processes in the EP, e.g., the thermocline feedback. This is the main reason that in the 1980s and 1990s the simulations and forecasts of ENSO utilizing the traditional models with an emphasis on the thermocline feedback are very successful. However, in the period of strong I (e.g., after 1999),

ignoring the effect of the zonal current has a strong negative impact on the ENSO simulations and forecasts.

7. Conclusions and Discussion

In this paper, an information-theoretic framework is developed to assess the predictability of complex chaotic systems in nature. The information theory advances a unique way to quantify the forecast uncertainty in exploring the predictability and allows to distinguish the predictability limit of each individual event in a complex system, which cannot be achieved by the traditional path-wise measurements. Understanding the gap between the intrinsic predictability and the prediction skill can provide potential guidelines to the improvement of the existing models and the current forecast methods. Such a study may also suggest that the efforts for further improving the forecast of certain types of the events is futile if they are inherently unpredictable. One of the most important steps in applying such a framework in practice is to build a statistically accurate dynamical model that can unbiasedly characterize the target phenomenon. Otherwise, the obtained information gain that represents the predictability may be polluted by the model errors.

The information-theoretic framework is then applied to quantifying the predictability of ENSO complexity, which includes different types of the ENSO events in both the EP and the CP regions with diverse characteristics in spatial pattern, peak intensity, and temporal evolution. While most of the conventional models focus on describing certain key dynamical properties of ENSO, a recently developed multiscale stochastic model succeeds in capturing both the large-scale dynamics and many crucial statistical properties of the observed ENSO complexity, including the PDFs, the seasonal phase-locking, the power spectrums and the ACFs of the SST in both the EP and CP regions. These desirable features allow the model to be a unique statistically accurate dynamical

system that facilitates the use of the information-theoretic framework to study the predictability of the ENSO complexity. Main conclusions are summarized as follows:

- [*Distinct predictability for different events*]. Different ENSO events possess very distinct predictability limits. Therefore, it is too crude to employ a single value of the predictability limit for the entire ENSO, as the path-wise measurements often do for assessing the ENSO forecast skill.
- [*Importance in both signal and dispersion*]. The CP SST T_C overall has more predictability than the EP SST T_E . Although the signal part dominates the total information gain in T_C , both the signal and dispersion parts have remarkable contributions to T_E . The latter indicates the importance of considering the entire forecast ensembles in characterizing the predictability instead of focusing on only the ensemble mean.
- [*No obvious spring barrier*]. The overall predictability starting from the spring season does not demonstrate any significant barrier. This indicates that if accurate and proper information can be obtained around spring, there might be a potential to make meaningful ENSO forecasts at long lead times, beyond the information provided by the climatology.
- [*EP El Niños*]. The information theory based predictability indicates that it is overall challenging to accurately predict the onset of the EP events, as the random wind bursts are one of its main triggering mechanisms. Both the predictability and the prediction skill may also differ significantly with a slight change of the starting date due to the rapid adjustment of the wind burst amplitude.
- [*CP El Niños*]. There seems to be a universal tendency that, starting from about 20 months in advance of a CP El Niño event, the time evolution of the information gain is always significant

at the timing of the target CP event. Remarkably, the strong predictability indeed converts to the skillful forecast for predicting many CP events about 2 years in advance.

- [*La Niñas*]. Stronger predictability is found in the La Niña events than both types of the El Niños, which is related to the more effective discharge process of ENSO at its mature stage.
- [*Climate change scenario*]. In the climate change scenario with the strengthening of the background Walker circulation, the predictability of T_C has a significant response with a notable increase in summer and fall. The predictability of T_E remains almost unchanged.
- [*Role of different variables*]. The loss of information becomes significant for predicting EP El Niño if the wind bursts are ignored and the main loss comes from the dispersion part, which is particularly detrimental to predicting the extreme events. The information loss in predicting T_C by excluding the wind is also notable in the signal part, which may lead to a mean bias in forecasting T_C . In contrast, the ocean zonal advection mainly affects the predicability of the CP El Niño. In addition, the decadal variability is important for improving the predictability of ENSO in both CP and EP regions.
- [*Justification of the Gaussian approximation*]. The Gaussian approximation is shown to be efficient and accurate in computing the information gain. Such a justification facilitates the use of the information theory to studying the ENSO predictability based on more sophisticated models, in which only a small number of the ensembles is affordable.

This paper presents a first step towards utilizing the information theory for understanding the predictability of the ENSO complexity. One practical task is to utilize the findings from the information-theoretic framework as the potential guidelines to improve the existing models and forecast methods. In particular, taking into account the potential predictability corresponding to the dispersion part deserves more emphasis in the model improvement. Another interesting topic is the

multi-model forecast, where the information theory can be used for the model selection that allows an optimal combination of different models to predict each type of the ENSO events. In addition, the exact initial conditions are used in the study of this paper. Yet, data assimilation is an essential step towards the practical forecast, which however will introduce additional uncertainty that may weaken the potential predictability. It is thus important to understand how data assimilation affects the predictability limit of the ENSO complexity and whether coupled atmosphere-ocean data assimilation is helpful in extending the predictability.

Acknowledgments. The research of X.F. is supported by Guangdong Major Project of Basic and Applied Basic Research (Grant No. 2020B0301030004), the Ministry of Science and Technology of the People's Republic of China (Grant No. 2020YFA0608802) and the National Natural Science Foundation of China (Grant No: 42192564). The research of N.C. is partially funded by the Office of VCRGE at UW-Madison and ONR N00014-21-1-2904.

Data availability statement. The monthly ocean temperature and current data were downloaded from GODAS (<https://www.esrl.noaa.gov/psd/data/gridded/data.godas.html>). The daily zonal wind data at 850 hPa were downloaded from the NCEP–NCAR reanalysis (<https://psl.noaa.gov/data/gridded/data.ncep.reanalysis.html>).

References

- Alexander, M. A., L. Matrosova, C. Penland, J. D. Scott, and P. Chang, 2008: Forecasting pacific ssts: Linear inverse model predictions of the PDO. *Journal of Climate*, **21** (2), 385–402.
- Ashok, K., S. K. Behera, S. A. Rao, H. Weng, and T. Yamagata, 2007: El Niño Modoki and its possible teleconnection. *Journal of Geophysical Research: Oceans*, **112** (C11).

- Barnston, A. G., M. K. Tippett, M. L. L'Heureux, S. Li, and D. G. DeWitt, 2012: Skill of real-time seasonal ENSO model predictions during 2002–11: Is our capability increasing? *Bulletin of the American Meteorological Society*, **93** (5), 631–651.
- Battisti, D. S., and A. C. Hirst, 1989: Interannual variability in a tropical atmosphere–ocean model: Influence of the basic state, ocean geometry and nonlinearity. *Journal of the Atmospheric Sciences*, **46** (12), 1687–1712.
- Behringer, D., and Y. Xue, 2004: Evaluation of the global ocean data assimilation system at NCEP: The Pacific Ocean. *Proc. Eighth Symp. on Integrated Observing and Assimilation Systems for Atmosphere, Oceans, and Land Surface*.
- Berner, J., and Coauthors, 2017: Stochastic parameterization: Toward a new view of weather and climate models. *Bulletin of the American Meteorological Society*, **98** (3), 565–588.
- Boucharel, J., R. Almar, E. Kestenare, and F.-F. Jin, 2021: On the influence of ENSO complexity on Pan-Pacific coastal wave extremes. *Proceedings of the National Academy of Sciences*, **118** (47).
- Branicki, M., N. Chen, and A. J. Majda, 2013: Non-Gaussian test models for prediction and state estimation with model errors. *Chinese Annals of Mathematics, Series B*, **34** (1), 29–64.
- Branstator, G., and H. Teng, 2010: Two limits of initial-value decadal predictability in a CGCM. *Journal of Climate*, **23** (23), 6292–6311.
- Buizza, R., and M. Leutbecher, 2015: The forecast skill horizon. *Quarterly Journal of the Royal Meteorological Society*, **141** (693), 3366–3382.
- Capotondi, A., and Coauthors, 2015: Understanding ENSO diversity. *Bulletin of the American Meteorological Society*, **96** (6), 921–938.

- Chen, D., and Coauthors, 2015: Strong influence of westerly wind bursts on El Niño diversity. *Nature Geoscience*, **8** (5), 339–345.
- Chen, N., X. Fang, and J.-Y. Yu, 2022: A multiscale model for El Niño complexity. *npj Climate and Atmospheric Science*, accepted.
- Chen, N., and A. J. Majda, 2016: Model error in filtering random compressible flows utilizing noisy Lagrangian tracers. *Monthly Weather Review*, **144** (11), 4037–4061.
- Chen, N., and A. J. Majda, 2018: Conditional gaussian systems for multiscale nonlinear stochastic systems: Prediction, state estimation and uncertainty quantification. *Entropy*, **20** (7), 509.
- Chen, N., A. J. Majda, and D. Giannakis, 2014a: Predicting the cloud patterns of the Madden-Julian Oscillation through a low-order nonlinear stochastic model. *Geophysical Research Letters*, **41** (15), 5612–5619.
- Chen, N., A. J. Majda, and X. T. Tong, 2014b: Information barriers for noisy Lagrangian tracers in filtering random incompressible flows. *Nonlinearity*, **27** (9), 2133.
- Christensen, H., J. Berner, D. R. Coleman, and T. Palmer, 2017: Stochastic parameterization and El Niño–Southern Oscillation. *Journal of Climate*, **30** (1), 17–38.
- Cover, T. M., 1999: *Elements of information theory*. John Wiley & Sons.
- DelSole, T., 2004: Predictability and information theory. Part I: Measures of predictability. *Journal of the Atmospheric Sciences*, **61** (20), 2425–2440.
- DelSole, T., 2005: Predictability and information theory. Part II: Imperfect forecasts. *Journal of the Atmospheric Sciences*, **62** (9), 3368–3381.

- DelSole, T., and M. K. Tippett, 2007: Predictability: Recent insights from information theory. *Reviews of Geophysics*, **45** (4).
- Dominiak, S., and P. Terray, 2005: Improvement of ENSO prediction using a linear regression model with a southern Indian Ocean sea surface temperature predictor. *Geophysical Research Letters*, **32** (18).
- Fang, X., and R. Xie, 2020: A brief review of ENSO theories and prediction. *Science China Earth Sciences*, **63** (4), 476–491.
- Fang, X., and F. Zheng, 2018: Simulating eastern-and central-pacific type ENSO using a simple coupled model. *Advances in Atmospheric Sciences*, **35** (6), 671–681.
- Fang, X.-H., and M. Mu, 2018: A three-region conceptual model for central Pacific El Niño including zonal advective feedback. *Journal of Climate*, **31** (13), 4965–4979.
- Fang, X.-H., and F. Zheng, 2021: Effect of the air–sea coupled system change on the ENSO evolution from boreal spring. *Climate Dynamics*, 1–12.
- Gardiner, C., 2009: *Stochastic methods*, Vol. 4. Springer Berlin.
- Giannakis, D., and A. J. Majda, 2012: Quantifying the predictive skill in long-range forecasting. Part II: Model error in coarse-grained markov models with application to ocean-circulation regimes. *Journal of Climate*, **25** (6), 1814–1826.
- Giannakis, D., A. J. Majda, and I. Horenko, 2012: Information theory, model error, and predictive skill of stochastic models for complex nonlinear systems. *Physica D: Nonlinear Phenomena*, **241** (20), 1735–1752.

- Gottwald, G. A., and J. Harlim, 2013: The role of additive and multiplicative noise in filtering complex dynamical systems. *Proceedings of the Royal Society A: Mathematical, Physical and Engineering Sciences*, **469** (2155), 20130096.
- Harrison, D., and G. A. Vecchi, 1997: Westerly wind events in the tropical pacific, 1986–95. *Journal of Climate*, **10** (12), 3131–3156.
- Hayashi, M., and M. Watanabe, 2017: ENSO complexity induced by state dependence of westerly wind events. *Journal of Climate*, **30** (9), 3401–3420.
- Hu, S., and A. V. Fedorov, 2016: Exceptionally strong easterly wind burst stalling El Niño of 2014. *Proceedings of the National Academy of Sciences*, **113** (8), 2005–2010.
- Jin, E. K., and Coauthors, 2008: Current status of ENSO prediction skill in coupled ocean–atmosphere models. *Climate Dynamics*, **31** (6), 647–664.
- Jin, F.-F., 1997: An equatorial ocean recharge paradigm for ENSO. Part I: Conceptual model. *Journal of the Atmospheric Sciences*, **54** (7), 811–829.
- Kalnay, E., and Coauthors, 1996: The NCEP/NCAR 40-year reanalysis project. *Bulletin of the American Meteorological Society*, **77** (3), 437–472.
- Kang, S. M., S.-P. Xie, Y. Shin, H. Kim, Y.-T. Hwang, M. F. Stuecker, B. Xiang, and M. Hawcroft, 2020: Walker circulation response to extratropical radiative forcing. *Science Advances*, **6** (47), eabd3021.
- Kao, H.-Y., and J.-Y. Yu, 2009: Contrasting eastern-Pacific and central-Pacific types of ENSO. *Journal of Climate*, **22** (3), 615–632.
- Kleeman, R., 2002: Measuring dynamical prediction utility using relative entropy. *Journal of the Atmospheric Sciences*, **59** (13), 2057–2072.

- Kleeman, R., 2011: Information theory and dynamical system predictability. *Entropy*, **13** (3), 612–649.
- Klein, S. A., B. J. Soden, and N.-C. Lau, 1999: Remote sea surface temperature variations during ENSO: Evidence for a tropical atmospheric bridge. *Journal of Climate*, **12** (4), 917–932.
- Kug, J.-S., F.-F. Jin, and S.-I. An, 2009: Two types of El Niño events: cold tongue El Niño and warm pool El Niño. *Journal of Climate*, **22** (6), 1499–1515.
- Kullback, S., 1959: Statistics and information theory. *J Wiley Sons, New York*.
- Kullback, S., 1987: Letter to the editor: The kullback-leibler distance. *AMERICAN STATISTICIAN*.
- Kullback, S., and R. A. Leibler, 1951: On information and sufficiency. *The Annals of Mathematical Statistics*, **22** (1), 79–86.
- Leeuwen, P., 2002: Balanced ocean-data assimilation near the equator. *Journal of Physical Oceanography*, **32**, 2509–2519.
- Liu, H., Y. Tang, D. Chen, and T. Lian, 2017: Predictability of the Indian Ocean Dipole in the coupled models. *Climate Dynamics*, **48** (5), 2005–2024.
- Majda, A., R. V. Abramov, and M. J. Grote, 2005: *Information theory and stochastics for multiscale nonlinear systems*, Vol. 25. American Mathematical Soc.
- Majda, A., R. Kleeman, D. Cai, and Coauthors, 2002: A mathematical framework for quantifying predictability through relative entropy. *Methods and Applications of Analysis*, **9** (3), 425–444.
- Majda, A. J., and N. Chen, 2018: Model error, information barriers, state estimation and prediction in complex multiscale systems. *Entropy*, **20** (9), 644.

- Majda, A. J., and D. Qi, 2018: Strategies for reduced-order models for predicting the statistical responses and uncertainty quantification in complex turbulent dynamical systems. *SIAM Review*, **60** (3), 491–549.
- McPhaden, M. J., S. E. Zebiak, and M. H. Glantz, 2006: ENSO as an integrating concept in earth science. *Science*, **314** (5806), 1740–1745.
- Neelin, J. D., and F.-F. Jin, 1993: Modes of interannual tropical ocean–atmosphere interaction—a unified view. Part II: Analytical results in the weak-coupling limit. *Journal of Atmospheric Sciences*, **50** (21), 3504–3522.
- Palmer, T. N., R. Buizza, F. Doblas-Reyes, T. Jung, M. Leutbecher, G. J. Shutts, M. Steinheimer, and A. Weisheimer, 2009: Stochastic parametrization and model uncertainty. *ECMWF Technical Memorandum*, **598**.
- Philander, S. G. H., 1983: El Niño Southern Oscillation phenomena. *Nature*, **302** (5906), 295–301.
- Picaut, J., M. Ioualalen, C. Menkès, T. Delcroix, and M. J. McPhaden, 1996: Mechanism of the zonal displacements of the pacific warm pool: Implications for ENSO. *Science*, **274** (5292), 1486–1489.
- Plant, R., and G. C. Craig, 2008: A stochastic parameterization for deep convection based on equilibrium statistics. *Journal of the Atmospheric Sciences*, **65** (1), 87–105.
- Planton, Y., J. Vialard, E. Guilyardi, M. Lengaigne, and T. Izumo, 2018: Western pacific oceanic heat content: A better predictor of La Niña than of El Niño. *Geophysical Research Letters*, **45** (18), 9824–9833.

- Puy, M., J. Vialard, M. Lengaigne, and E. Guilyardi, 2016: Modulation of equatorial Pacific westerly/easterly wind events by the Madden–Julian oscillation and convectively-coupled Rossby waves. *Climate Dynamics*, **46 (7-8)**, 2155–2178.
- Ren, H.-L., J. Zuo, and Y. Deng, 2019: Statistical predictability of niño indices for two types of ENSO. *Climate Dynamics*, **52 (9)**, 5361–5382.
- Ropelewski, C. F., and M. S. Halpert, 1987: Global and regional scale precipitation patterns associated with the El Niño/Southern Oscillation. *Monthly Weather Review*, **115 (8)**, 1606–1626.
- Sapsis, T. P., and A. J. Majda, 2013: Statistically accurate low-order models for uncertainty quantification in turbulent dynamical systems. *Proceedings of the National Academy of Sciences*, **110 (34)**, 13 705–13 710.
- Schopf, P. S., and M. J. Suarez, 1988: Vacillations in a coupled ocean–atmosphere model. *Journal of Atmospheric Sciences*, **45 (3)**, 549–566.
- Stein, K., A. Timmermann, N. Schneider, F.-F. Jin, and M. F. Stuecker, 2014: ENSO seasonal synchronization theory. *Journal of Climate*, **27 (14)**, 5285–5310.
- Tang, Y., R. Kleeman, and A. M. Moore, 2005: Reliability of ENSO dynamical predictions. *Journal of the Atmospheric Sciences*, **62 (6)**, 1770–1791.
- Tang, Y., H. Lin, J. Derome, and M. K. Tippett, 2007: A predictability measure applied to seasonal predictions of the Arctic Oscillation. *Journal of Climate*, **20 (18)**, 4733–4750.
- Teng, H., and G. Branstator, 2011: Initial-value predictability of prominent modes of North Pacific subsurface temperature in a CGCM. *Climate Dynamics*, **36 (9-10)**, 1813–1834.

- Thual, S., A. J. Majda, and N. Chen, 2019: Statistical occurrence and mechanisms of the 2014–2016 delayed super El Niño captured by a simple dynamical model. *Climate Dynamics*, **52** (3-4), 2351–2366.
- Thual, S., A. J. Majda, N. Chen, and S. N. Stechmann, 2016: Simple stochastic model for El Niño with westerly wind bursts. *Proceedings of the National Academy of Sciences*, **113** (37), 10245–10250.
- Timmermann, A., and Coauthors, 2018: El Niño–Southern Oscillation complexity. *Nature*, **559** (7715), 535–545.
- Tziperman, E., and L. Yu, 2007: Quantifying the dependence of westerly wind bursts on the large-scale tropical Pacific SST. *Journal of Climate*, **20** (12), 2760–2768.
- Tziperman, E., S. E. Zebiak, and M. A. Cane, 1997: Mechanisms of seasonal–ENSO interaction. *Journal of the Atmospheric Sciences*, **54** (1), 61–71.
- Wang, B., X. Luo, Y.-M. Yang, W. Sun, M. A. Cane, W. Cai, S.-W. Yeh, and J. Liu, 2019: Historical change of El Niño properties sheds light on future changes of extreme El Niño. *Proceedings of the National Academy of Sciences*, **116** (45), 22512–22517.
- Wang, C., and J. Picaut, 2004: Understanding ENSO physics—A review. *Earth’s Climate: The Ocean–Atmosphere Interaction, Geophys. Monogr.*, **147**, 21–48.
- Wang, L., H.-L. Ren, J. Zhu, and B. Huang, 2020: Improving prediction of two ENSO types using a multi-model ensemble based on stepwise pattern projection model. *Climate Dynamics*, **54** (7), 3229–3243.
- Xie, R., and X. Fang, 2020: The unusual 2014–2016 El Niño events: Dynamics, prediction and enlightenments. *Science China Earth Sciences*, **63** (5), 626–633.

- Yang, Q., A. J. Majda, and N. Chen, 2021: ENSO diversity in a tropical stochastic skeleton model for the MJO, El Niño, and dynamic Walker circulation. *Journal of Climate*, 1–56.
- Yu, J.-Y., and H.-Y. Kao, 2007: Decadal changes of ENSO persistence barrier in SST and ocean heat content indices: 1958–2001. *Journal of Geophysical Research: Atmospheres*, **112 (D13)**.
- Zebiak, S. E., and M. A. Cane, 1987: A model El Niño–Southern Oscillation. *Monthly Weather Review*, **115 (10)**, 2262–2278.
- Zhang, R.-H., S. E. Zebiak, R. Kleeman, and N. Keenlyside, 2003: A new intermediate coupled model for El Niño simulation and prediction. *Geophysical Research Letters*, **30 (19)**.

LIST OF TABLES

Table 1. Summary of the non-dimensional units and the model parameters. 47

TABLE 1. Summary of the non-dimensional units and the model parameters.

$[h]$	150 m	$[T]$	7.5°C
$[u]$	1.5 m/s	$[t]$	2 months
$[\tau]$	5 m/s	d_τ	2
γ	0.75	r	0.25
α_1	0.0625	α_2	0.125
b_0	2.5	μ	0.5
σ	$0.2I$	λ	0.1
$p(I)$	$0.25 \text{ in } I \in (0, 4)$	c_U	0.03
$\Phi(x)$	$\int_b^x (y-m)p(y)dy$	$\sigma_I(I)$	$\sqrt{\frac{2}{p(I)}} [-\lambda\Phi(I)]$
β_E	$0.15(2-0.2I)$	β_u	$-0.2\beta_E$
β_h	$-0.4\beta_E$	β_C	$0.8\beta_E$
σ_u	0.04	σ_h	0.02
σ_C	0.04	σ_E	0
$\sigma_\tau(T_C, t)$	$0.9[\tanh(7.5T_C) + 1] \left[1 + 0.3 \cos\left(\frac{2\pi}{6}t + \frac{2\pi}{6}\right) \right]$		
$c_1(T_C, t)$	$\left[25\left(T_C + \frac{0.75}{7.5}\right)^2 + 0.9 \right] \left[1 + 0.3 \sin\left(\frac{2\pi}{6}t - \frac{2\pi}{6}\right) \right]$		
$c_2(t)$	$1.4 \left[1 + 0.2 \sin\left(\frac{2\pi}{6}t + \frac{2\pi}{6}\right) + 0.15 \sin\left(\frac{2\pi}{3}t + \frac{2\pi}{6}\right) \right]$		

LIST OF FIGURES

Fig. 1.	Schematic illustration of quantifying the predictability of complex natural phenomena using information theory.	50
Fig. 2.	Comparison of the spatiotemporal patterns and the statistics between the observations and the coupled multiscale stochastic model. Panel (a) is the SST anomalies along the equatorial Pacific during 1980-2020. Panel (b) is same as (a) but is the random selected period during model year 230-270. Panels (c) and (d) are power spectrums of Niño3 and Niño4 SST, respectively. Panels (e) and (f) are PDFs. Panels (g) and (h) are the monthly variance (i.e., the seasonal cycle). Panels (i) and (j) are the ACF. In each panel, red and blue curves are for the observation and model, respectively. For the model, the total 2000-year long simulation is divided into 50 non-overlapping segments, each of which has a 40-year period as the observation. Then the average (blue line) and its one standard deviation intervals (shading) are illustrated.	51
Fig. 3.	Prediction error measured for the observation (1982–2019) and 54 non-overlapping segments of the model years with the same length. For each segment and the observation, 100 members are used to perform the ensemble prediction for every month with a lead time from 1 to 12 months . Then, the ensemble mean of the predictions is used to calculate the RMSE with the target. The number in the title of each subplot indicates the lead time in months. The value for the observation is plotted with a longer bar. The mean and standard deviation of the statistics obtained from the segments are represented by the horizontal error bars.	52
Fig. 4.	The information gain of the T_E as a function of the starting date (x-axis) and the lead (y-axis). Panel (a) shows the total information gain based on the non-Gaussian PDFs. Panel (b) is the information gain computed based on the Gaussian approximations. Panels (c) and (d) show the signal and dispersion components of the information gain, respectively. The solid red line, purple line and blue line at the top of each panel represents EP El Niño, CP El Niño and La Niña years, respectively.	53
Fig. 5.	Similar to Figure 4 but for T_C	54
Fig. 6.	The information gain as a function of the starting month. Panels (a)–(c) are for T_E and panels (d)–(f) are for T_C	55
Fig. 7.	The information gain in predicting T_E and T_C as a function of the starting month for EP El Niño, CP El Niño and La Niña. The top, middle and bottom rows illustrate the total information gain, the signal part and the dispersion part, respectively. In each panel, the black and red lines are the information gain in predicting T_E and T_C , respectively.	56
Fig. 8.	The total information gain in predicting T_E and T_C for a moderate EP El Niño event (1986-1988), a super El Niño event (1997-1998) and the delayed super El Niño event (2014-2016). The two white solid lines provide the time window within which the corresponding event is active.	57
Fig. 9.	The initial values of different variables for the ensemble forecasts of super El Niños in 1997 and 2015.	58
Fig. 10.	Prediction of the 2015-2016 super El Niño. The first row shows the ensemble forecast of T_E , where the ensemble members are shown in blue curves and the ensemble mean is in green. It is compared with the true event, which is in black. The red and pink shading areas indicate the one and two standard deviations of the climatological PDF. The second row shows the	

percentile that the true event lies within the PDF of the ensemble forecast (blue) and that of the climatology (pink). The third and the fourth rows are similar but for T_C . The four columns show the ensemble forecasts starting from different months: (a) March, (b) April, (c) May, and (d) June. 59

Fig. 11. Hovmoller diagram of the ensemble forecast for the 2015-2016 super El Niño. Column (a) is the true observed event. Column (b) and (c) show the best and the worst ensemble forecast member, respectively. Column (d) shows the ensemble mean forecast. Different rows show the forecast starting from different months, as marked by the black dashed-dot line. The values before the black dashed-dot line have been set to be zero. The pink dashed line is the dateline. 60

Fig. 12. The total information gain in predicting T_E and T_C for an isolated CP Niño event (2004-2005) and a mixed CP-EP event (2009-2010). The two white solid lines provide the time window within which the corresponding event is active. 61

Fig. 13. Information gain in predicting T_C for different CP El Niño events. Panel (a) shows the Hovmoller diagram of the observed SST anomaly. Six CP or CP-EP mixed El Niño events are marked next to the Hovmoller diagram. Panels (b)–(g) show the information gain of T_C for each of these events. The black dashed boxes inside some of these panels indicate the significant information gain at around 20 months lead time. Panels (h)–(j) show the ensemble forecasts for three of those six events, where the black bar at the top of each panel marks the time span of the corresponding CP El Niño event. 62

Fig. 14. The total information gain in predicting T_E and T_C for a single year La Niña event (1988-1989) and a multi-year La Niña event (1998-2001). The two white solid lines provide the time window within which the corresponding event is active. 63

Fig. 15. Ensemble forecast of the 1998-2001 multi-year La Niña and the 2004-2005 isolated CP El Niño. The blue curves show the 50 randomly selected ensemble members with the ensemble mean being green. The true observed event is shown in black color. The red and pink shading areas show the one and two standard deviations of the climatology distribution. 64

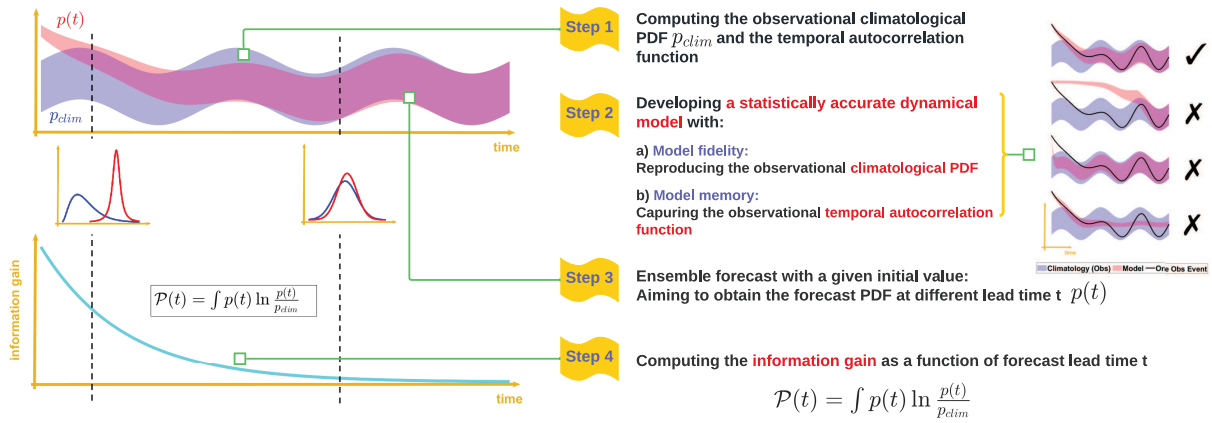
Fig. 16. ENSO predictability in the climate change scenarios using the twin experiments. Panel (a) shows the number of different ENSO events occurred per 70 years. The bar indicates the confidence interval based on 30 independent model simulations, each of which is 70 years long as the observations from 1950 to 2020. Panels (b)–(d) show the information gain in predicting T_E (black) and T_C (red) using the standard model run, the model with $I = 0$ and the model with $I = 4$. Here the threshold value $\mathcal{E} = 0.2$ of the information gain in (4) is used for comparison. 65

Fig. 17. The information loss in predicting T_E (Column (a)) and in predicting T_C (Column (b)) due to the ignorance of the intraseasonal zonal wind stress τ 66

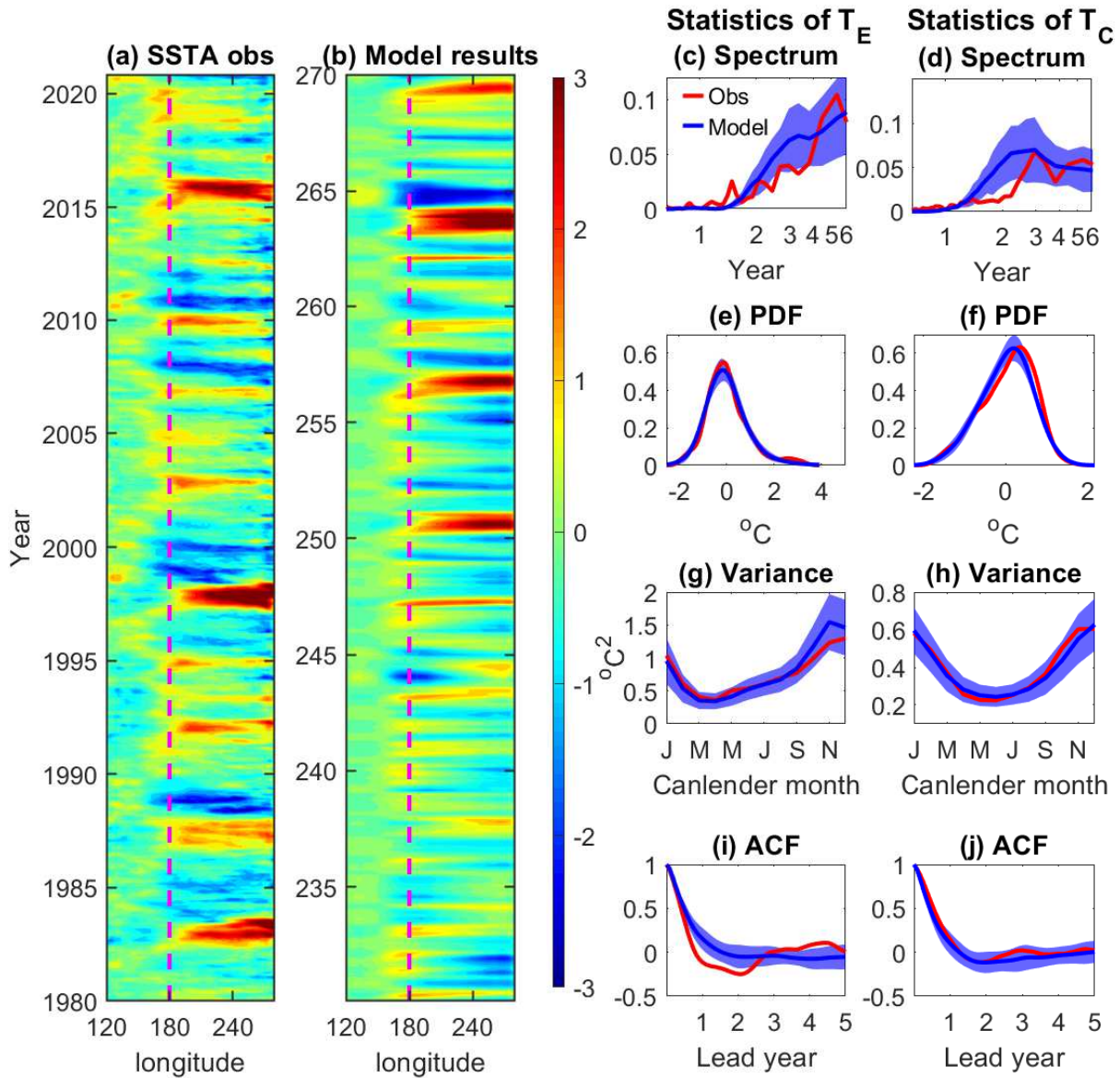
Fig. 18. The information loss in predicting T_E (Panel (a)) and in predicting T_C (Panel (b)) due to the ignorance of the decadal variability I . For reference, the observed I is shown in Panel (c). 67

Fig. 19. The information loss in predicting T_E (Panel (a)) and in predicting T_C (Panel (b)) due to the ignorance of the ocean current u . For reference, the observed u together with the observed I are shown in Panels (c) and (d). 68

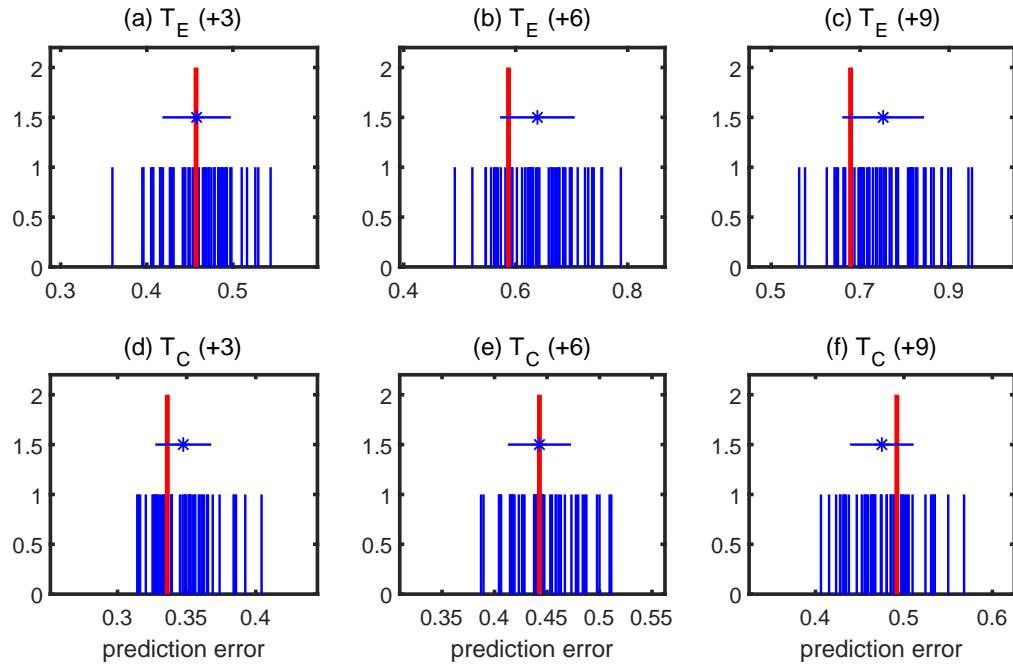
Quantifying the Predictability of Complex Natural Phenomena Using Information Theory



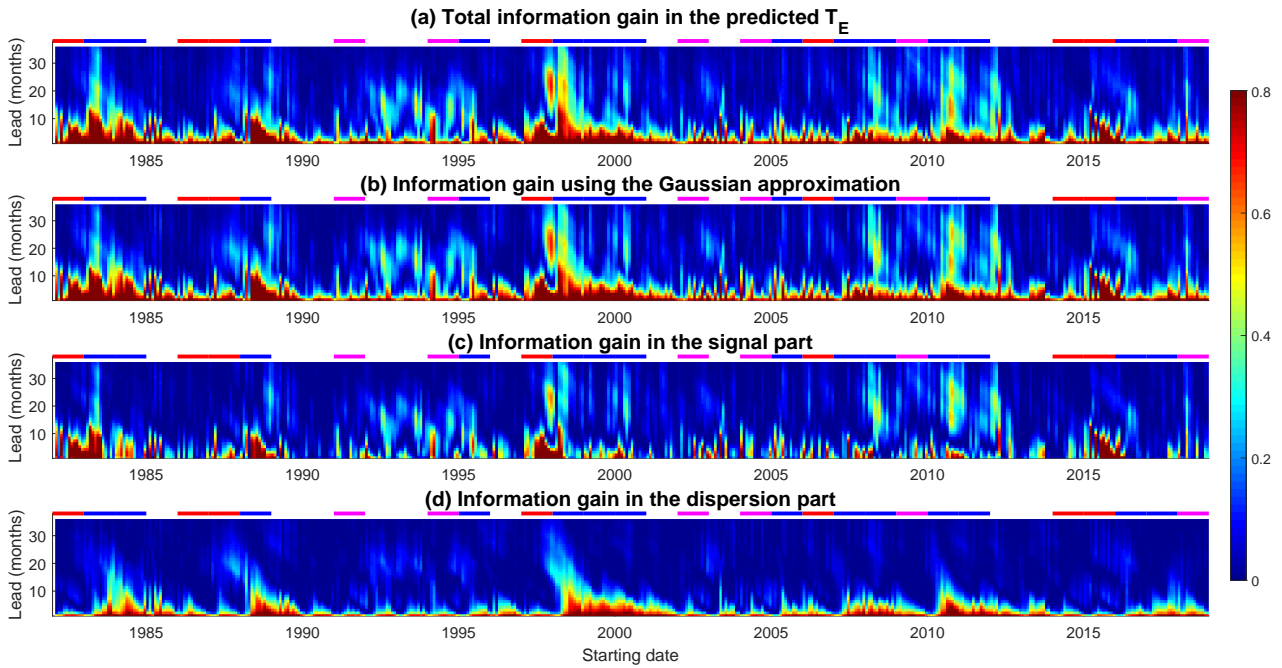
26 FIG. 1. Schematic illustration of quantifying the predictability of complex natural phenomena using information
 27 theory.



28 FIG. 2. Comparison of the spatiotemporal patterns and the statistics between the observations and the coupled
 29 multiscale stochastic model. Panel (a) is the SST anomalies along the equatorial Pacific during 1980-2020. Panel
 30 (b) is same as (a) but is the random selected period during model year 230-270. Panels (c) and (d) are power
 31 spectrums of Niño3 and Niño4 SST, respectively. Panels (e) and (f) are PDFs. Panels (g) and (h) are the monthly
 32 variance (i.e., the seasonal cycle). Panels (i) and (j) are the ACF. In each panel, red and blue curves are for
 33 the observation and model, respectively. For the model, the total 2000-year long simulation is divided into 50
 34 non-overlapping segments, each of which has a 40-year period as the observation. Then the average (blue line)
 35 and its one standard deviation intervals (shading) are illustrated.



36 FIG. 3. Prediction error measured for the observation (1982–2019) and 54 non-overlapping segments of the
 37 model years with the same length. For each segment and the observation, 100 members are used to perform the
 38 ensemble prediction for every month with a lead time from 1 to 12 months . Then, the ensemble mean of the
 39 predictions is used to calculate the RMSE with the target. The number in the title of each subplot indicates the
 40 lead time in months. The value for the observation is plotted with a longer bar. The mean and standard deviation
 41 of the statistics obtained from the segments are represented by the horizontal error bars.



42 FIG. 4. The information gain of the T_E as a function of the starting date (x-axis) and the lead (y-axis). Panel (a)
 43 shows the total information gain based on the non-Gaussian PDFs. Panel (b) is the information gain computed
 44 based on the Gaussian approximations. Panels (c) and (d) show the signal and dispersion components of the
 45 information gain, respectively. The solid red line, purple line and blue line at the top of each panel represents EP
 46 El Niño, CP El Niño and La Niña years, respectively.

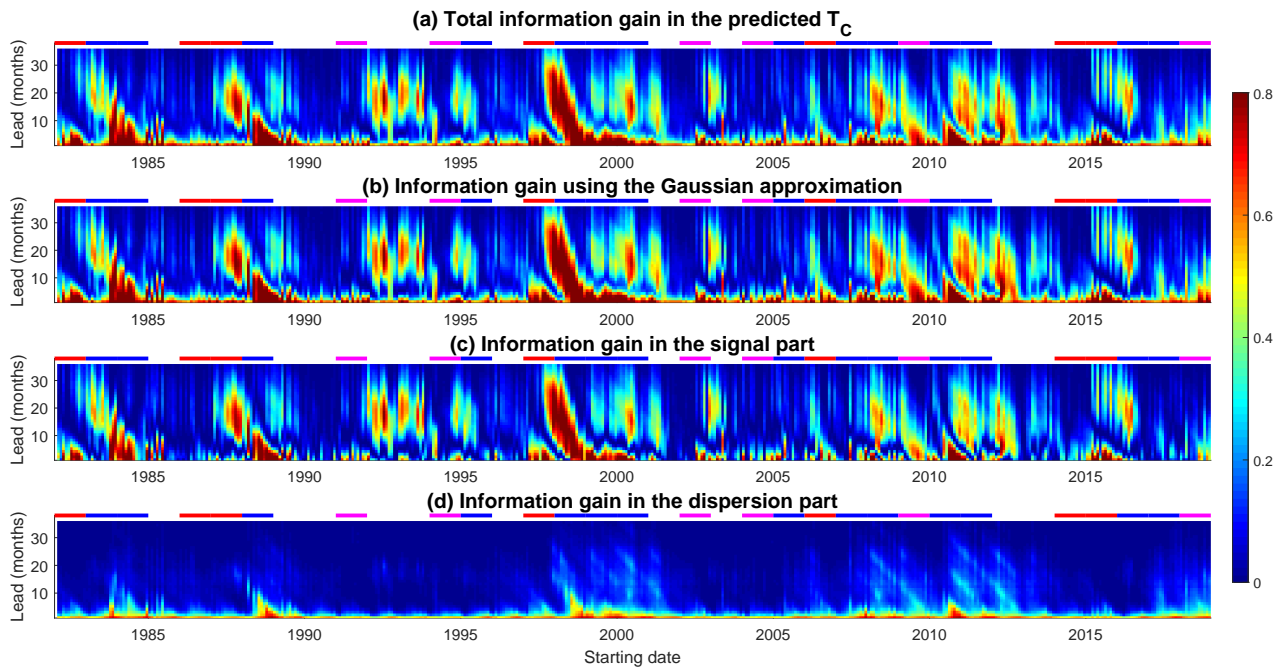
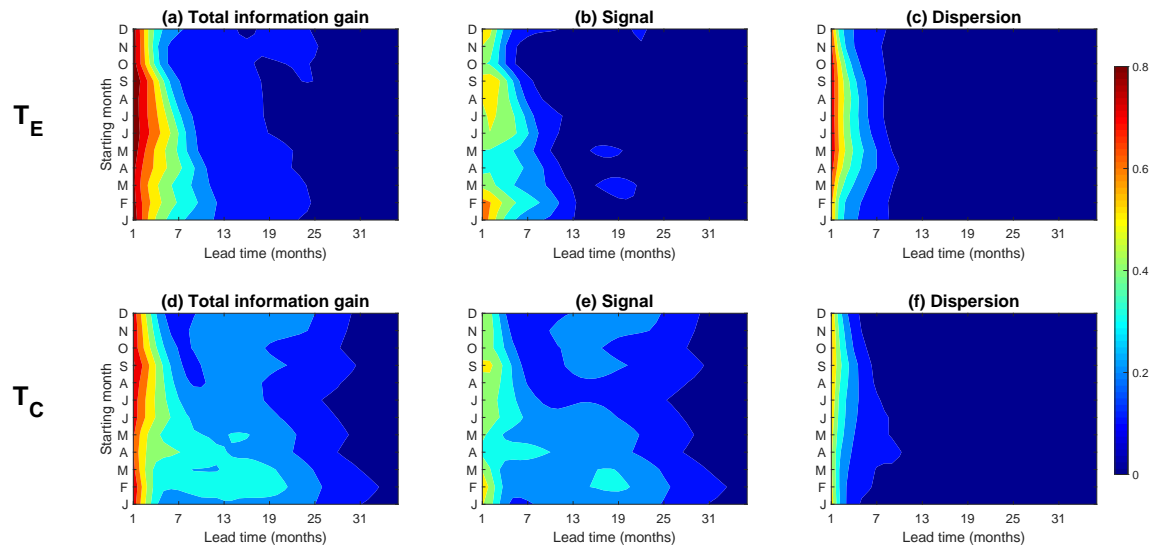
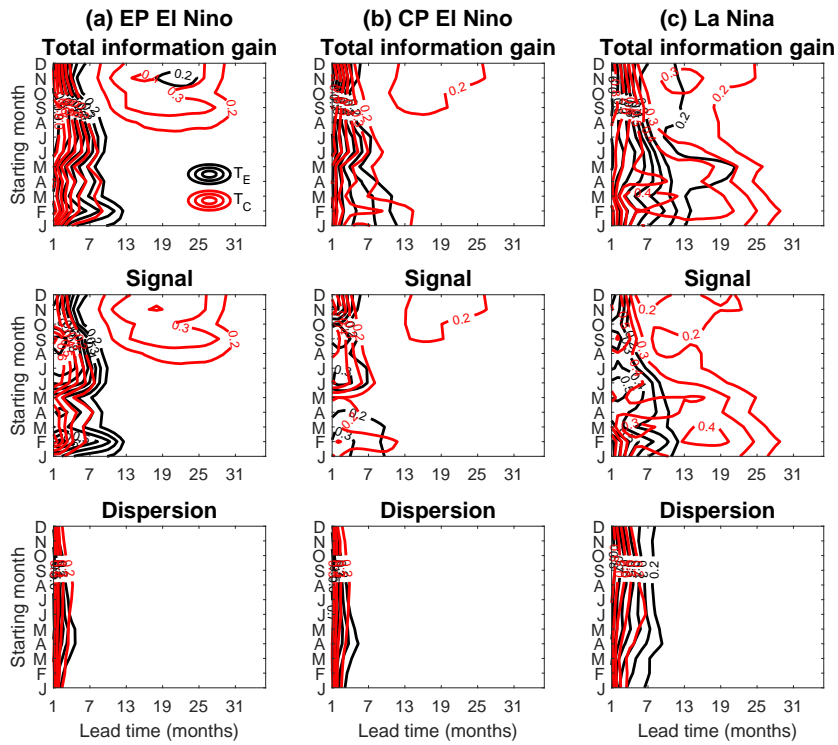


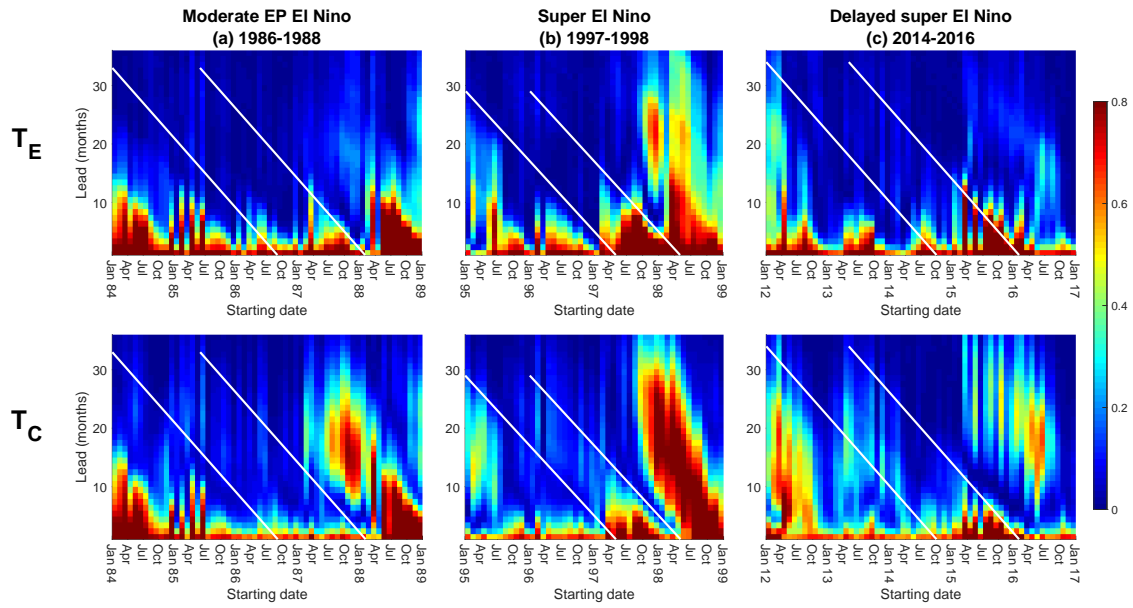
FIG. 5. Similar to Figure 4 but for T_C .



47 FIG. 6. The information gain as a function of the starting month. Panels (a)–(c) are for T_E and panels (d)–(f)
 48 are for T_C .



49 FIG. 7. The information gain in predicting T_E and T_C as a function of the starting month for EP El Niño, CP
 50 El Niño and La Niña. The top, middle and bottom rows illustrate the total information gain, the signal part and
 51 the dispersion part, respectively. In each panel, the black and red lines are the information gain in predicting T_E
 52 and T_C , respectively.



53 FIG. 8. The total information gain in predicting T_E and T_C for a moderate EP El Niño event (1986-1988), a
 54 super El Niño event (1997-1998) and the delayed super El Niño event (2014-2016). The two white solid lines
 55 provide the time window within which the corresponding event is active.

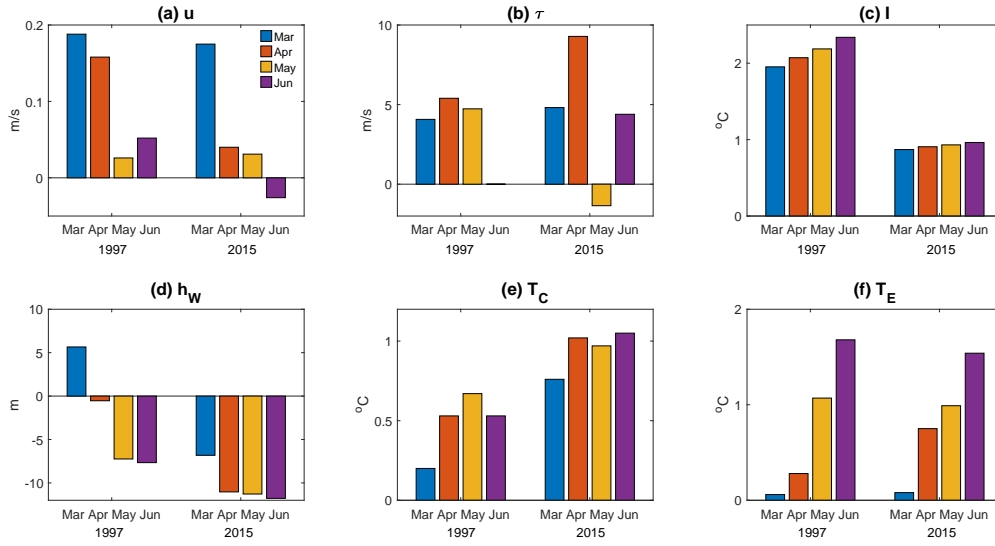
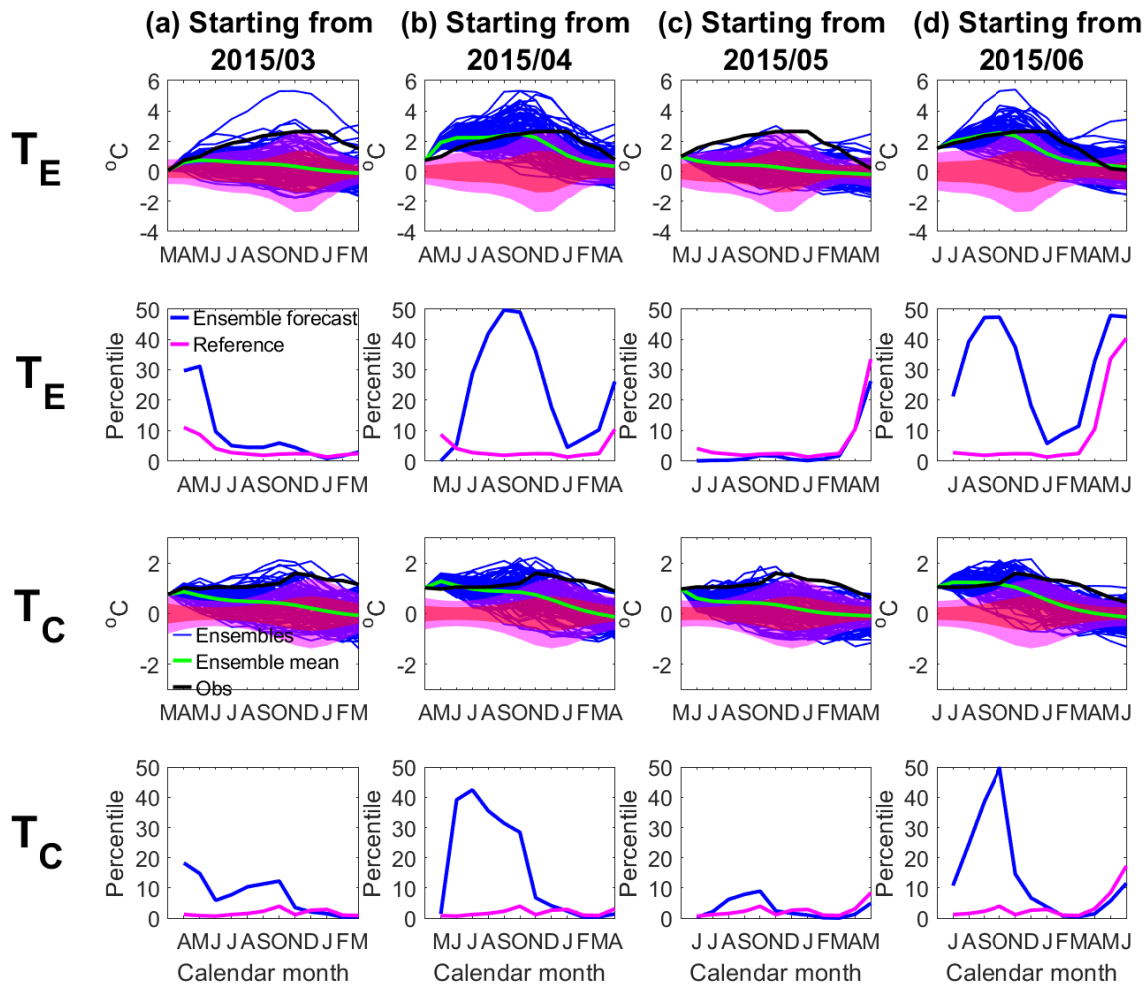
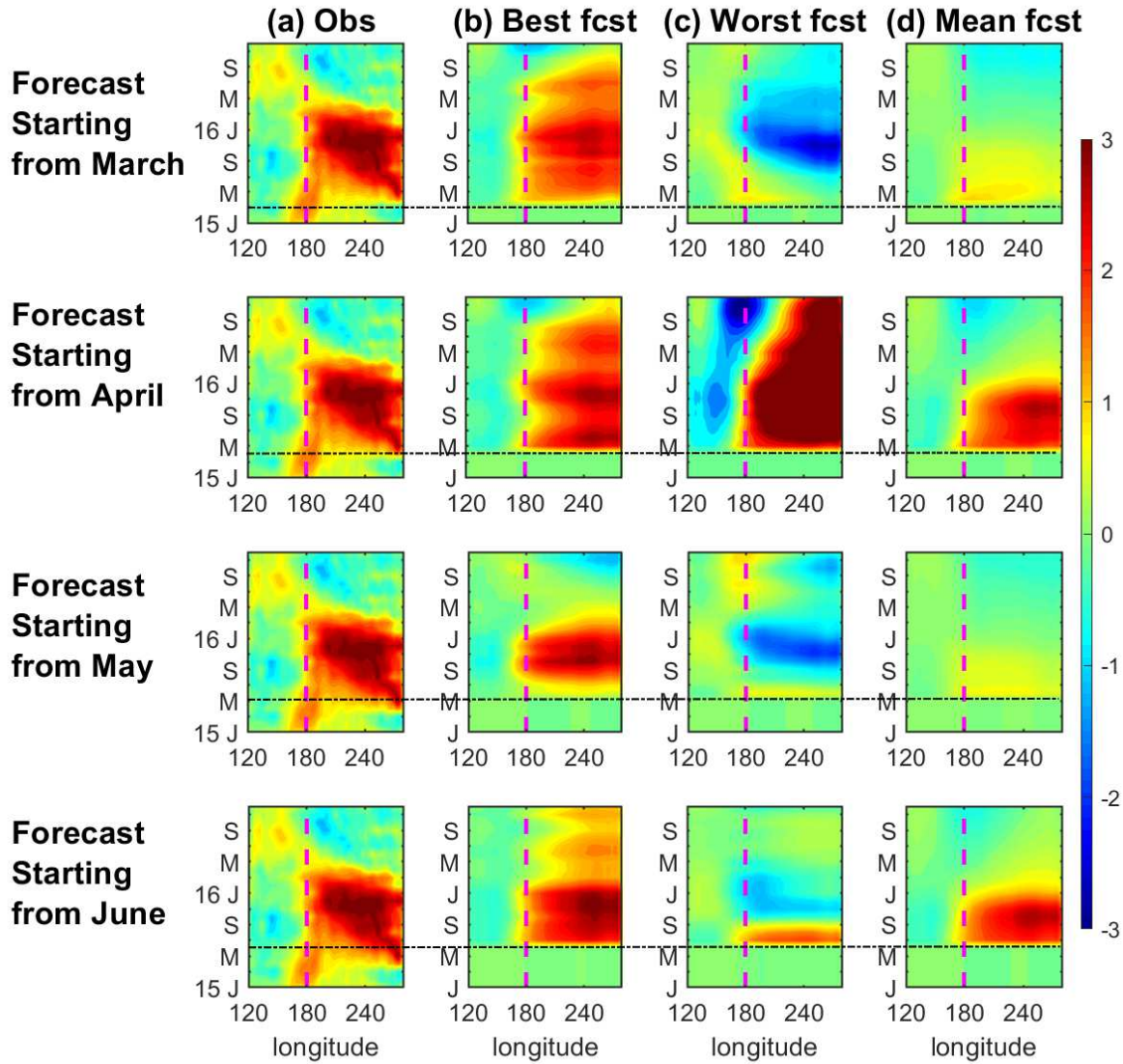


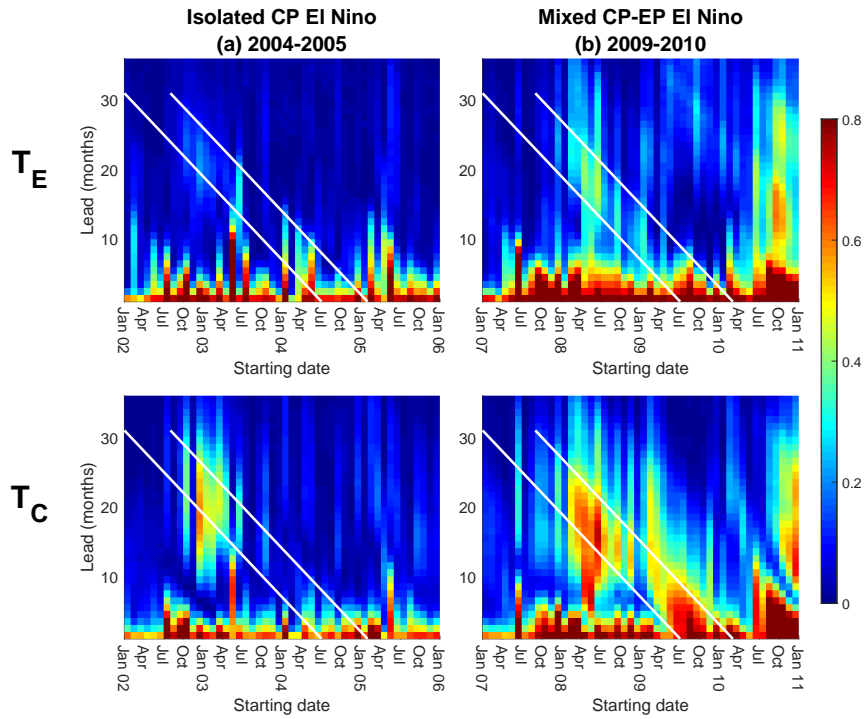
FIG. 9. The initial values of different variables for the ensemble forecasts of super El Niños in 1997 and 2015.



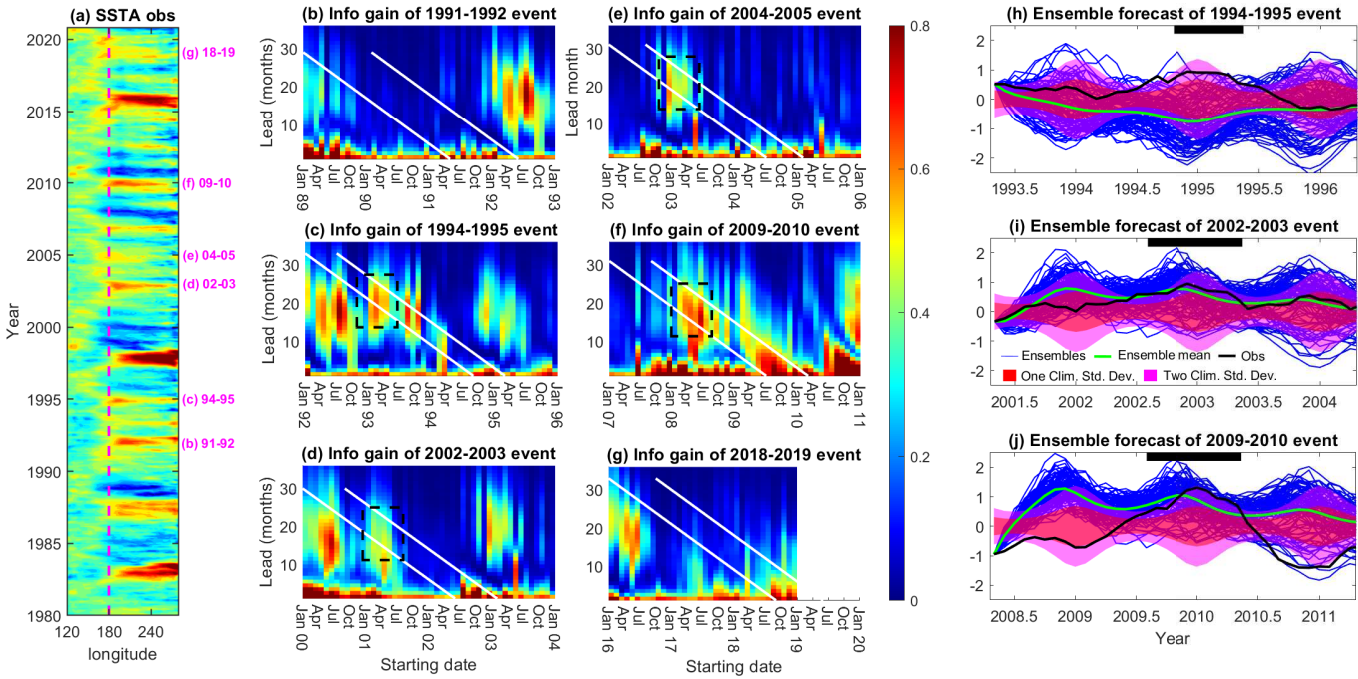
56 FIG. 10. Prediction of the 2015-2016 super El Niño. The first row shows the ensemble forecast of T_E , where
 57 the ensemble members are shown in blue curves and the ensemble mean is in green. It is compared with the
 58 true event, which is in black. The red and pink shading areas indicate the one and two standard deviations of the
 59 climatological PDF. The second row shows the percentile that the true event lies within the PDF of the ensemble
 60 forecast (blue) and that of the climatology (pink). The third and the fourth rows are similar but for T_C . The four
 61 columns show the ensemble forecasts starting from different months: (a) March, (b) April, (c) May, and (d) June.



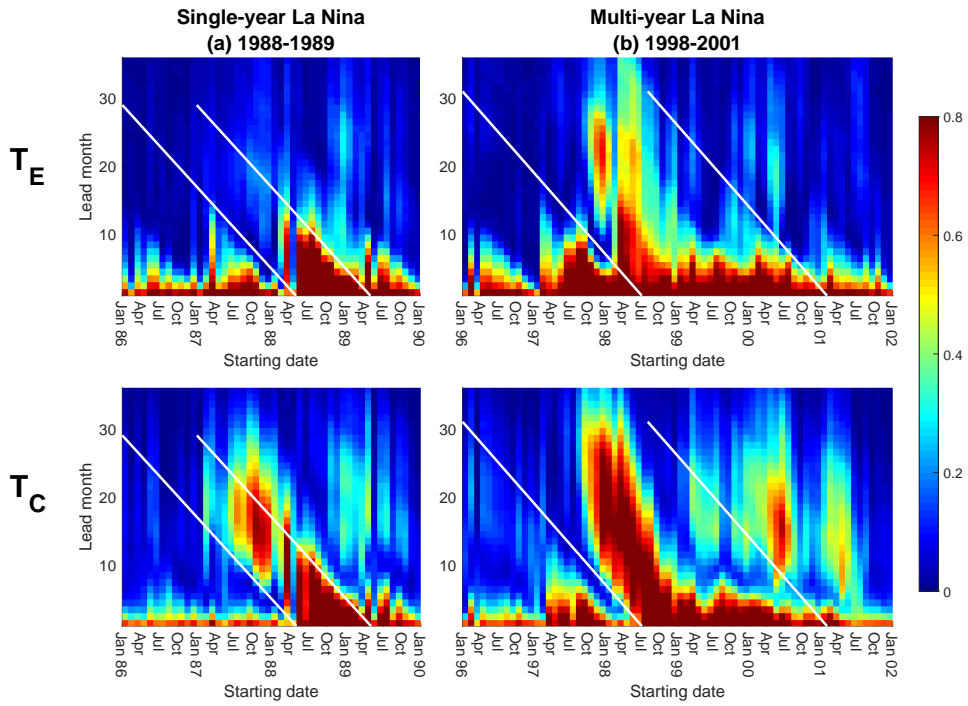
62 FIG. 11. Hovmoller diagram of the ensemble forecast for the 2015-2016 super El Niño. Column (a) is the
 63 true observed event. Column (b) and (c) show the best and the worst ensemble forecast member, respectively.
 64 Column (d) shows the ensemble mean forecast. Different rows show the forecast starting from different months,
 65 as marked by the black dashed-dot line. The values before the black dashed-dot line have been set to be zero.
 66 The pink dashed line is the dateline.



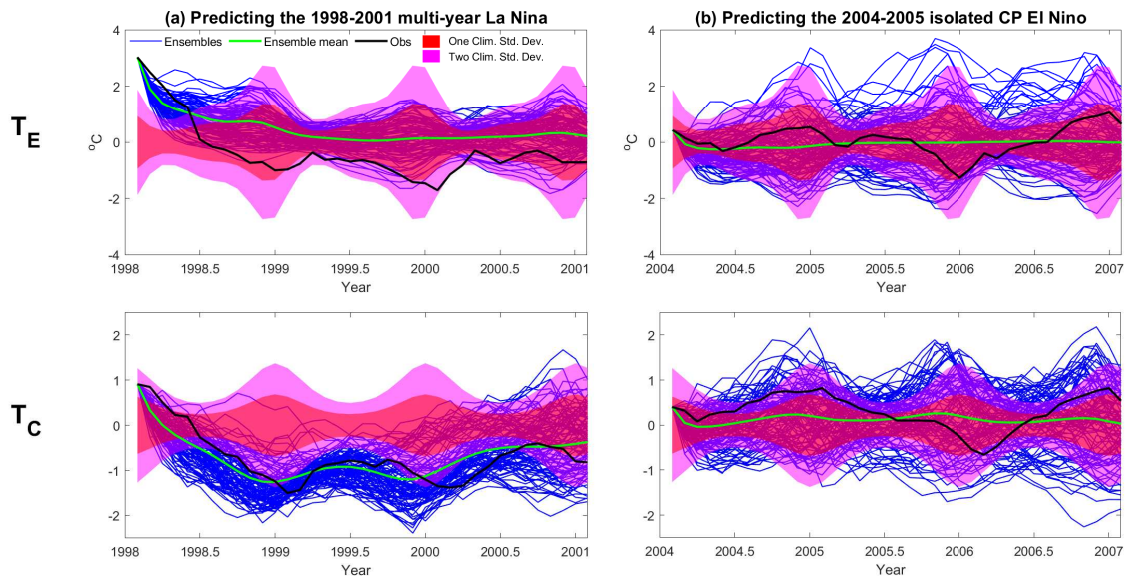
67 FIG. 12. The total information gain in predicting T_E and T_C for an isolated CP Niño event (2004-2005)
 68 and a mixed CP-EP event (2009-2010). The two white solid lines provide the time window within which the
 69 corresponding event is active.



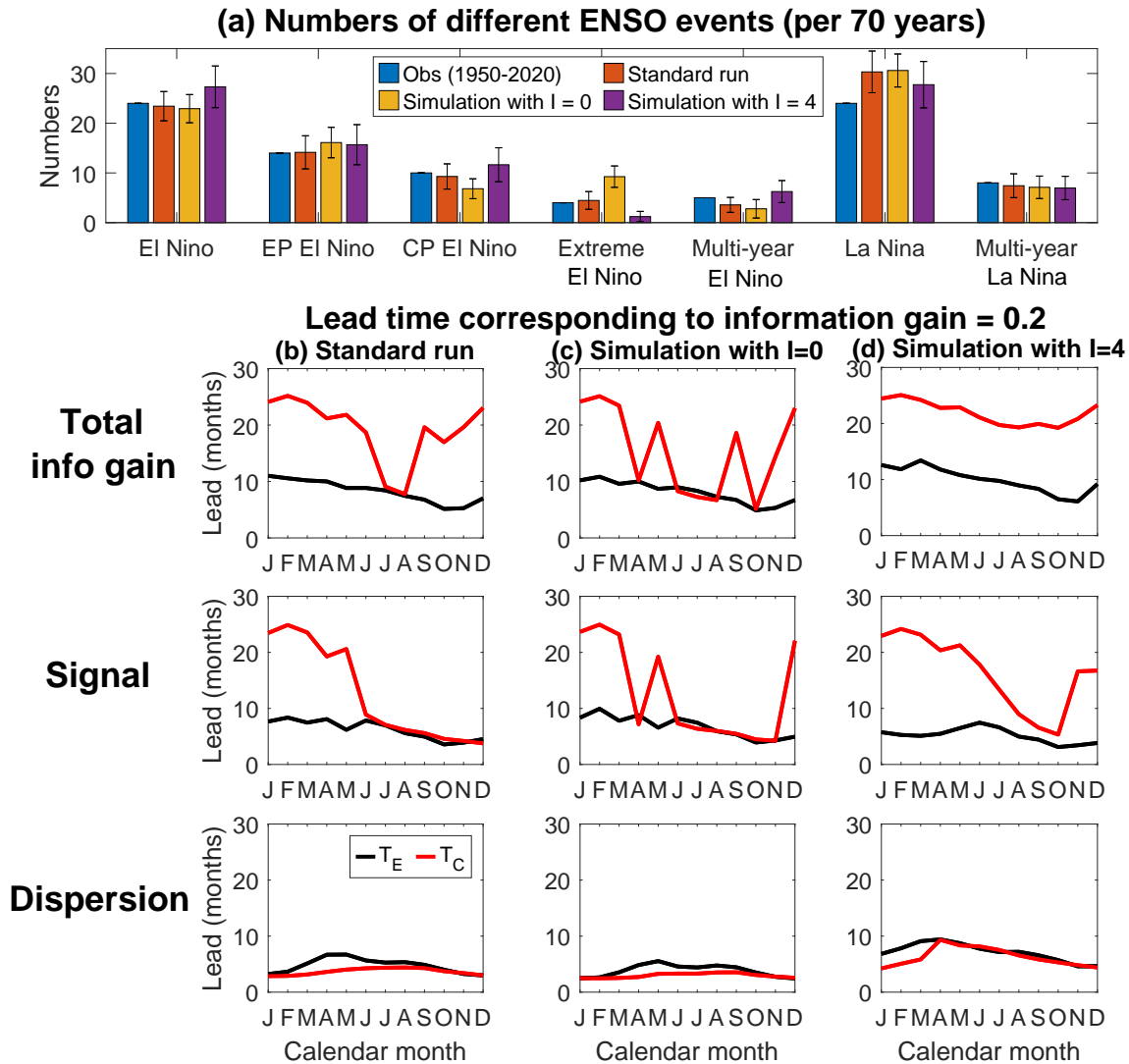
70 FIG. 13. Information gain in predicting T_C for different CP El Niño events. Panel (a) shows the Hovmoller
 71 diagram of the observed SST anomaly. Six CP or CP-EP mixed El Niño events are marked next to the Hovmoller
 72 diagram. Panels (b)–(g) show the information gain of T_C for each of these events. The black dashed boxes inside
 73 some of these panels indicate the significant information gain at around 20 months lead time. Panels (h)–(j) show
 74 the ensemble forecasts for three of those six events, where the black bar at the top of each panel marks the time
 75 span of the corresponding CP El Niño event.



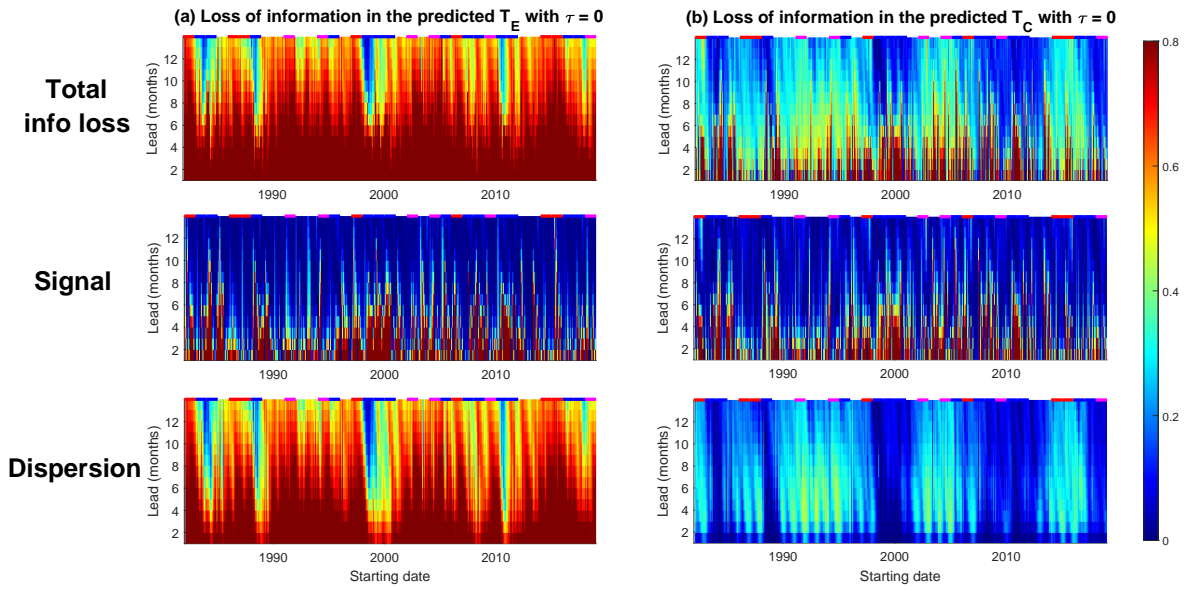
76 FIG. 14. The total information gain in predicting T_E and T_C for a single year La Niña event (1988-1989) and
 77 a multi-year La Niña event (1998-2001). The two white solid lines provide the time window within which the
 78 corresponding event is active.



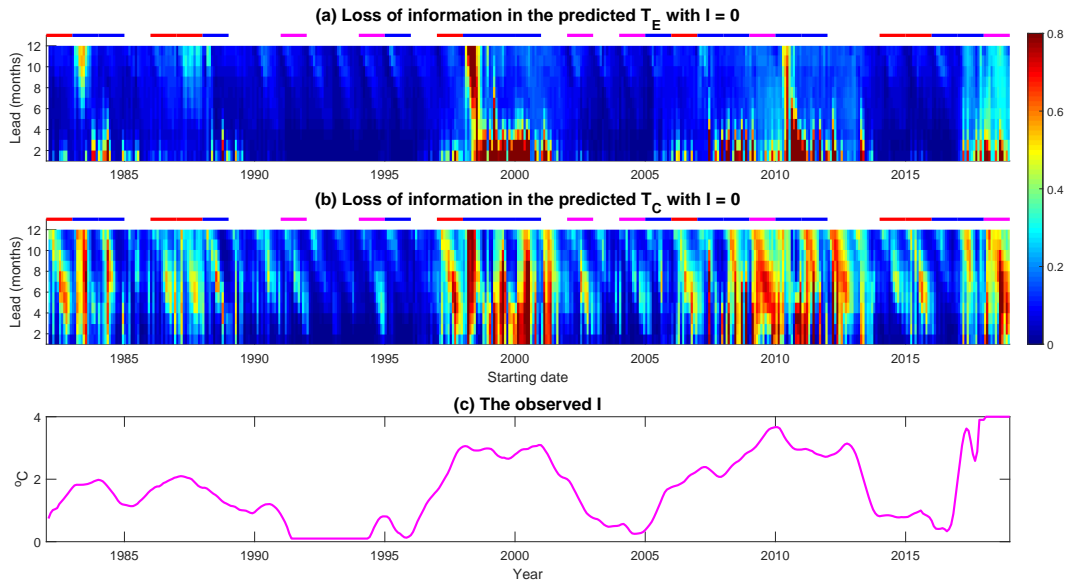
79 FIG. 15. Ensemble forecast of the 1998-2001 multi-year La Niña and the 2004-2005 isolated CP El Niño. The
 80 blue curves show the 50 randomly selected ensemble members with the ensemble mean being green. The true
 81 observed event is shown in black color. The red and pink shading areas show the one and two standard deviations
 82 of the climatology distribution.



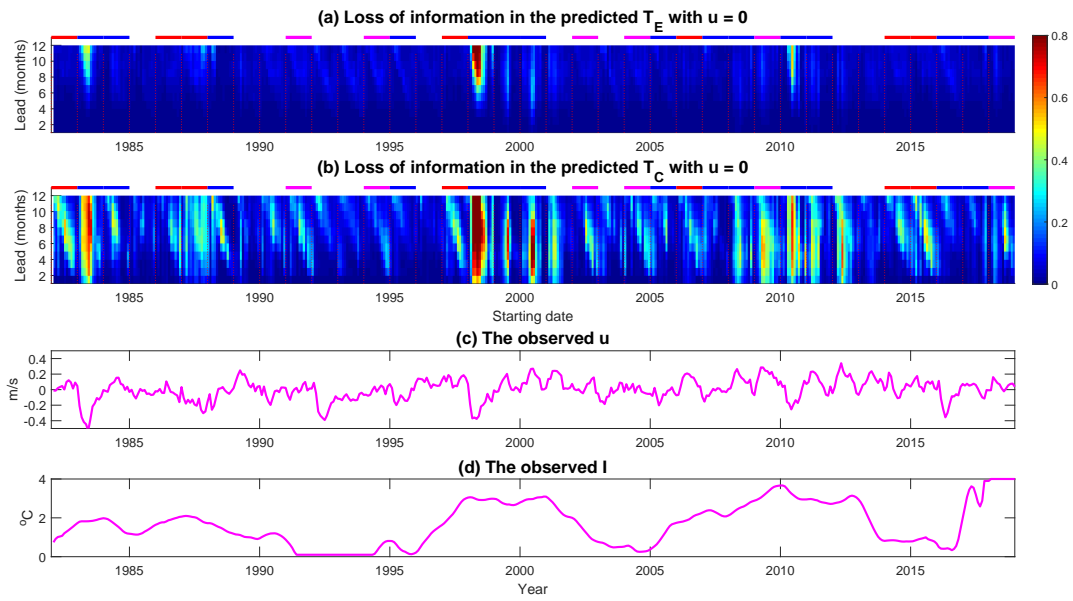
83 FIG. 16. ENSO predictability in the climate change scenarios using the twin experiments. Panel (a) shows the
 84 number of different ENSO events occurred per 70 years. The bar indicates the confidence interval based on 30
 85 independent model simulations, each of which is 70 years long as the observations from 1950 to 2020. Panels
 86 (b)–(d) show the information gain in predicting T_E (black) and T_C (red) using the standard model run, the model
 87 with $I = 0$ and the model with $I = 4$. Here the threshold value $\mathcal{E} = 0.2$ of the information gain in (4) is used for
 88 comparison.



89 FIG. 17. The information loss in predicting T_E (Column (a)) and in predicting T_C (Column (b)) due to the
 90 ignorance of the intraseasonal zonal wind stress τ .



91 FIG. 18. The information loss in predicting T_E (Panel (a)) and in predicting T_C (Panel (b)) due to the ignorance
 92 of the decadal variability I . For reference, the observed I is shown in Panel (c).



93 FIG. 19. The information loss in predicting T_E (Panel (a)) and in predicting T_C (Panel (b)) due to the ignorance
 94 of the ocean current u . For reference, the observed u together with the observed I are shown in Panels (c) and
 95 (d).